Journal of Civil Structural Health Monitoring (2023) 13:827–866
https://doi.org/10.1007/s13349-022-00667-0

ORIGINAL PAPER

Proof load testing and shear assessment of kishwaukee I-39-river bridge using the modified compression field theory

Alain Saroufim[1] · Moussa A. Issa[2] · Mohammad Mahdi[1] · Mohsen A. Issa[1]

Received: 22 August 2022 / Accepted: 24 December 2022 / Published online: 16 March 2023

Abstract

The questions raised about bridge performance are carried out by conducting physical bridge load testing and rating. The outcomes of bridge load testing are widely used to ensure bridge safety for the public when theoretical analysis cannot provide a sufficient conclusion of in-service performance. The research illustrates the load ratings and shear assessment of a 1976-built I-39 Kishwaukee bridge over the Kishwaukee River in Winnebago County, District 1, Illinois. Load ratings of the Kishwaukee twin post-tensioned concrete box girder bridges are governed mainly by the shear stresses located near the piers in combination with visible shear cracks exhibited at the joints around the shear key due to the inception of the cracks at the time of construction in single key joints. Proof of four different trucks loading weights of 76 tons (167 k), 90 tons (200 k), 122 tons (268 k), and 136 tons (300 k) were conducted on the bridge. Nine testing scenarios were successfully completed with a maximum of two testing trucks of approximately 136 tons (300 k). Half of the bridge was instrumented using vibrating wire strain gauges to measure the strains near the pier, where shear and negative moment are critical, and at midspan, where the positive moment is crucial. Furthermore, crackmeters were placed along the cracks near the shear key region to measure the crack opening during testing. Linear variable differential transducers (LVDTs) were placed at the critical Sect. (0.40L) of Span #5 to measure the deflection. The modified compression field theory (MCFT) is used to calculate the shear capacity along the joints considering the contributions of vertical and horizontal reinforcing steel, the prestressing Dywidag bars, and the effect of the external post-tension tendons. This paper illustrates a detailed procedure for Kishwaukee Bridge load rating, field operation, instrumentation, and interpretation of the test results to determine the bridge load rating based on the 2018 AASHTO Manual for Bridge Evaluation. Findings from this study demonstrated that there is no crack slippage across the web-cracked section, and the bridge's concrete shear capacity remains strong and contributes to the bridge's total shear capacity. This study also showed that the shear capacity of the bridge is 1.8 times stronger than the total applied shear force, concluding that the Kishwaukee I-39 bridge remains safe for future traffic load increases or higher truck loads.

Keywords Kishwaukee I39-river bridge · Precast post-tensioned box girders · Proof load testing · Bridge load rating · Modified compression field theory

List of symbols

A_{ps}	Area of prestressed longitudinal reinforcement on the flexural tension side of a member
A_s	Area of the non prestressed steel on the flexural tension side of the member = 0 in^2(only prestressing steel is used)
A_v	Area of shear reinforcement within distance s
A_{ct}	Concrete tension area
$\alpha 1$	Tendon angle near the pier
$\alpha 2$	Tendon angle near the pier
α	Angle of inclination of transverse reinforcement to the longitudinal axis.
a_{max}	Maximum aggregate size

✉ Moussa A. Issa
moussa.issa@hbmengineering.com

Alain Saroufim
alain.saroufim@hotmail.com

Mohammad Mahdi
mohammad.mahdi.0491@gmail.com

Mohsen A. Issa
missa@uic.edu

[1] University of Illinois at Chicago, Chicago, IL, USA

[2] HBM Engineering Group, LLC, Hillside, USA

b_v	Effective web width taken as the minimum web width within the depth d_v
β	Tensile stress factor indicating the ability of cracked concrete to transmit tension and shear
β_{DL}	Load combination coefficient for dead loads
β_{LL}	Load combination coefficient for live loads
d_v	Effective shear depth taken as the distance of $0.72 \times h$ eight of the section
D	Dead load
E_s	Modulus of elasticity of reinforcing bars
E_p	Modulus of elasticity of prestressing tendons
E_c	Modulus of elasticity of concrete
f'_c	Concrete compressive strength
F_{cr}	Concrete cracking strength
F_p	Shear force calculated in each cable
f_{pu}	Ultimate stress of presstressing strand
f_{po}	Parameter taken as modulus of elasticity of prestressing steel multiplied by the locked-in difference in strain between the prestressing steel and the concrete surrounding.
f_y	Steel reinforcement yield strength
f_1	Average principal tensile stress in the concrete
f_v	Tensile stress in the shear reinforcement
I	Impact load
K	Portion factor
K_1	Aggregate correction factor
L	Live load
L_c	Distance between the cracks
L_T	Target proof load
$Losses$	Losses due to shrinkage, creep and relaxation
M_u	Factored moment at the section
N_u	Calculated factored axial load at the section
s	spacing of the transverse reinforcement measured in a direction parallel to the longitudinal reinforcement
V_n	Nominal shear strength
V_p	Vertical component of the prestressing force
η_{tendon}	Number of tendons on one side of the bridge
η_{strand}	Number of prestressing strands per conduit
V_c	Nominal shear strength in concrete
V	Combined concrete and reinforcement shear capacity
V_{nMCFT}	Bridge shear capacity derived from the MCFT
V_u	Factored shear force
ϕV_n	Design shear strength
V_s	Nominal shear strength provided by shear reinforcement
$V_{u,1w}$	Total applied shear force on single web
$V_{LL,1w}$	Shear force due to live load one single web
$V_{DL,1w}$	Shear force due to dead load on single web
ϕV_{n_MCFT}	Bridge design shear capacity derived from the MCFT
v_{ci}	Local shear stress at the crack
$v_{ci\_allowable}$	Maximum allowable local shear stress at the crack
$v_{ci\_}$	Calculated local shear stress at the crack on site
w	Crack width measured
θ	Angle of inclination of diagonal compressive stresses
σ	Stress in the concrete
ε	Strain in the concrete
ε_1	Strain collected from the strain gauges at the crack
λ	Concrete density modification factor
ε_s	Net longitudinal tensile strain in the section at the centroid of the tension reinforcement concrete
γ	Load factor applied to all loads

1 Introduction

Many countries worldwide face a common problem with the aging bridge infrastructure that is being demanded to carry increasing loads [1]. With the cost and the difficulties associated with replacing and rehabilitating these bridges, it is necessary to make the most efficient use of the existing infrastructure [1]. In 2010, the Federal Highway Administration (FHWA) stated that 50 billion miles of travel road increase were recorded yearly from 1985 to 2008 [2]. In 1998, the trucks in the United States (US) delivered 77% of the total freight weight, and in 2010 the FHWA showed that around 79% of goods weight and 84% by value in the US are transported by trucks using the interstate highway system [2]. This continuous rise in truck loading weight accelerates the deterioration of highway bridges and decreases their life expectancy. Since the interstate highway sector is vital to the country's economy, the bridge load ratings procedures and investigation should accurately reflect the bridge load capacity condition, especially the old ones [3]. Bridge load ratings are necessary for new and old constructed bridges that need maintenance and to check the appropriateness of the structure members to ensure minimum safety under the effect of future traffic loads [4]. When the collapse of the Silver Bridge in West Virginia occurred in 1967, the catalyst resulted in the establishment of the National Bridge Inspection Standards (NBIS) [5]. The NBIS demanded all states to carry out bridge inspections every 2 years and the inspection data should be reported to the National Bridge Inventory. The NBIS data showed that out of 600,000 bridges in the US, more than 50% are classified as deficient [5].

On August 1, 2007, the I-35 W Mississippi River bridge collapsed in Minnesota, and it sparked immediate calls all over the US to investigate, repair, or replace the nation's aging infrastructure [6]. This unexpected failure

prompted the responsible authorities to inspect and evaluate the bridge's load-carrying capacity more accurately [7]. The bridge load rating through load testing shows that a bridge has an additional capacity well beyond the traditional analysis or can uncover stress spiking, unexpected deflection, or crack initiation causing the end of the loading test [7]. The outcomes of the bridge load testing method contribute to develop a field-verified finite element models (FEM) [8, 9], evaluating the material damage evolution on the bridge performance [10], assessment of strengthening measures [11–13] and bridges evaluation without designs plans [14–17]. The improvement in the technology of Internet of Things (IoT) concerning sensors, data acquisitions systems, and cellular communications for sensing, gathering, and storing the data in conjunction with finite element modeling has resulted in combining analytical models and field tests for better assessment of the bridge condition [8]. The AASHTO 2016 code combined the concept of structure reliability with the applied proof loads in the current provision for load testing given in Chapter 8 of the AASHTO Manual for Bridge Evaluation. Therefore, based on the rating results, a decision can be taken as to whether the bridge is in good condition, if it needs maintenance, or may remain in service with a posted weight limit [3].

2 Background

The Kishwaukee River Bridge, located on I-39 about 4 miles south of Rockford, Illinois, is a twin post-tensioned segmental concrete box girder bridge. The construction began in the mid-70 s and was completed in 1980 [18]. The twin box girders were made from precast concrete and erected using the balanced cantilever method [19]. The Kishwaukee Bridge is considered the first project in the United States where the launching truss method in construction is used [19]. The bridge consists of five (5) spans with an overall length of approximately 1170 ft (357 m) distributed as follows: three interior spans of 250 ft (76.2 m) each and two end spans of 170 ft (51.8 m) each [19] as shown in Fig. 1. In the mid-70 s, the segmental structures were still inaugural in the United States, and the design was based on a single shear-key joint located around the centroid of the cross-section [18], as shown in Fig. 2.

During the construction of the south-bound bridge, cracks, and slippage appeared at the shear key between the pier segment and the cantilever adjacent segment [19]. The distress behavior in the bridge was the consequence of nonhardened epoxy at the joints, which is supposed to carry most of the shear stresses. In contrast, the nonhardened epoxy acted as a lubricant and canceled all the concrete friction forces at the joint's surface. Since most of the stresses were concentrated at the shear key, the cracks occurred in the female part of the joint between the pier segment and the cantilever adjacent to it [19]. A retrofit was carried out before traffic opening in 1982, consisting of implementing stainless steel dowels along the shear key and through the web thickness, allowing the shear to transfer through the bearing sides of the dowels [19].

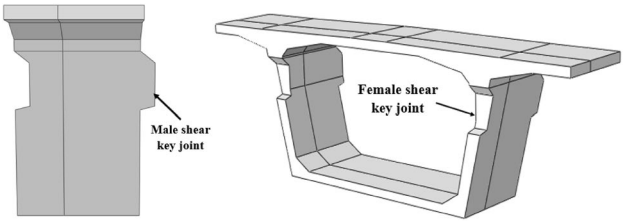

Fig. 2 Isometric view of I-39 Kishwaukee bridge segment

In early 2000, the box girder webs in both north and south-bound bridges continued to express continuous cracking and deterioration [20]. A structural investigation of the bridge determined that the crack growth along the webs is caused by principal tensile stresses higher than the code limits [20]. To reduce the shear forces acting across the webs, engineers strengthened the structure using external post-tensioning tendons placed inside the box girders. Four-12 strands, 15 mm post-tensioned tendons with their deviators, were placed inside the box girder cell, and the resulting implementation turned out to be effective.

In 2018, the bridge was inspected by the HBM engineering group, and the rating report showed that the segment near the piers might have a possible crack propagation and that a physical rating of the bridge is necessary to better understand it's behavior. Therefore, performing a physical static load testing of the bridge is vital and can accurately determine the amount of the reserve capacity, especially with all attempts to police loads, overweight vehicles are still using the bridges every day [21]. Moreover, higher loads are expected in the future, and one needs to know the actual safe load that these bridges can carry [21].

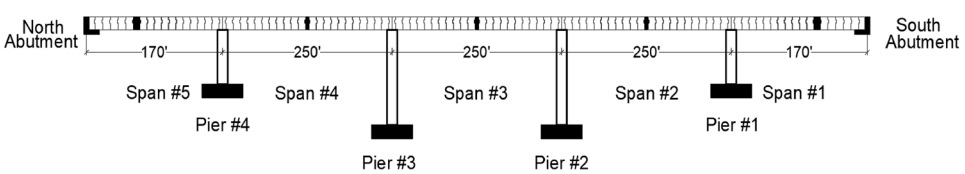

Fig. 1 I-39-Kishwaukee river bridge elevation view

2.1 Related work and testing objective

The bridge load rating is a technique to test and evaluate the bridge's various structural components' adequacy to carry a predetermined live load [22]. Bridge load physical testing proved to be a reliable method to assess the bridge and reflect its actual behavior and physical condition [23]. Based on AASHTO, The Manual Bridge for Evaluation [24], bridge load rating can be realized based on the Diagnostic Load Test (DLT) or Proof Load Testing (PLT). A DLT is based on determining the specific behavior of the bridge under a specific load and validating the results using the analytical model [25]. Both methods rely on data obtained from field measurement parameters and the structural response of the bridge during the test [26]. The PLT test consists of applying a target load to prove directly that a bridge is able to carry at least the live loads recommended by the AASHTO code in addition to a magnified vehicular load, mainly trucks [24]. PLT determines the maximum safe load capacity of the bridge by increasing the load incrementally until a specific load is achieved or a non-linear behavior is observed [23]. In PLT, instrumentation and monitoring equipment are placed on points of maximum response (critical locations) where potential failure may occur [21]. Faber et al. [27], state that a proof load rating is very successful in demonstrating the bridge resistance, controlling the bridge age, increasing the bridge testing reliability, and reducing uncertainties due to the assumptions made for bridges without documentation. The results from proof load testing are vital in developing a field-verified finite element model since the test outcomes can be used to calibrate the analytical model [25]. Moreover, many highway bridges are aging and lack documentation. In the absence of reinforcement plans and documentation, conservative assumptions are made for the reinforcement details and concrete properties for the analysis [15]. As a result, the bridge load rating using the analytical method is not possible, and proof load rating is the only method left to evaluate the bridge [28].

Recently, analytical assessment of the bridge has been commonly used, but theoretical analysis often leads to a conservative estimation of bridge capacity. Factors such as load distribution, composite action, material properties, unintended continuity, and end restraint are challenging to model accurately, resulting in a higher strength than that generated from the theoretical analysis [1]. The load applied in a PLT is generally two to three times the legal load level allowing the dynamic, fatigue and overload effect to be accounted for when rating the bridge [1]. The Proof Load Testing procedure does not change significantly worldwide, but the magnitude of the applied loads and load factors used to calculate the load rating vary. Ransom et al., rated the South Pine River Bridge built in 1941. The bridge is six spans simply supported bridge located in Brisbane, Australia [1]. The testing was broken into seven load increments to reach a target proof load of 106 Tons. The authors demonstrated that the experimentally measured strains are about 65% of the value of the theoretical strain induced from the same applied load [1]. In Ontario, Canada, the Ministry of Transportation has a long history of bridge assessment using the PLT method. The country has proof tested more than 225 bridges since the bridge assessment program started in 1969 [29]. The loads applied are according to the ultimate limit state live load of the Ontario Highway Bridge Design Code. Bakht and Jaeger, in 1990, demonstrated from the proof load tested bridge in Ontario that these bridges have reserves strength not shown by the theoretical analysis [29]. In Switzerland, The Federal and Cantonal Administration requires that new bridges are always proof tested before they are commissioned for service [30]. Moses et al., in 1994, described the load tests conducted on bridges in Switzerland as 'Acceptance Proof Test' and are mainly used to quantify the overall behavior of the structure [31]. The main objective of proof loading in Switzerland was to ensure that the bridge demonstrates a linear behavior under the applied load and that the measured displacements are fully recoverable. However, according to Favre et al. in 1992, the total applied loads on the structure are approximately 250 kN (56 kips) per vehicle which is significantly lower than the target loads applied in other countries [30].

Several bridges are rated each year in the US, but publications regarding this topic are mainly restricted to significant bridges. Comisu et al., developed an intelligent system for durability assessment based on data collected from inspection and long-term monitoring of bridges. The model combines the visual inspection parameters with the stored data to build a realistic foreseeing deterioration model [32]. In 2002, Coletti et al. [33], instrumented the Roma-Ciudad Miguel Aleman International Suspension Bridge in Texas, USA. The author measured the deflection of the bridge under proof loadings and developed a field FEM for future analytical study of the bridge under heavier loads. Chen et al., monitored the Hurley Bridge (Wisconsin Structure B-26-7) from April 2010 till June 2011. The authors analyzed the strain and deflection data obtained from the monitoring system and developed a statistical approach that links the bridge performance and statical process control for better management of transportation infrastructure [34]. Zhou et al., in 2020, inspected the I-195 westbound of Washington Bridge over the Seekonk River in Rhode Island, built in 1967. The bridge consisted of 13 prestressed concrete girder spans and five steel plate girder spans. The authors instrumented one span using 32 strain gauge sensors to evaluate the effect of shear at the dapped end of the girder under different loading stages to verify the linear elastic behavior [35]. The testing results proved that the bridge load rating showed a higher level of

reliability than the analytical diagnostic of the bridge since it reduces the assumptions made when calculating the structural capacity using conventional methods. In addition, the I-195 Bridge rating proved that the actual shear capacity of the bridge is much higher than the analytical method, which undermines the actual shear capacity of the bridge. In 2015, Anay et al., monitored a prestressed concrete bridge in southern New Mexico. The bridge was 40 years old, and no design plans were available. The bridge was instrumented using Acoustic Emission (AE) sensors and tested under proof loading. Based on the analysis of the AE data, the authors demonstrated that the bridge showed signs of microcracks development near the supports where the shear is critical and in the midspan where the positive moment controls [15]. Jauregui et al., in 2004, conducted a DLT test on the prestressed concrete girder I-40 Bridge over the Rio Grande River in Albuquerque. The authors used the outcomes from the DLT and the finite element analysis to rate the bridge capacity and concluded that the I-40 Bridge could be safely increased by a factor of 1.7 [17]. Lloyd et al. [36] monitored Kishwaukee I39-Bridge for a long time to determine the structure state and crack propagation and provide the necessary information for any retrofit operation needed to increase the bridge's lifetime.

Also, it is understood that most structures properly designed under AASHTO specifications will have relatively large amounts of reserve strength or overstrength. Although the use of AASHTO load factors is based on statistical analysis and loading probability, the usage of "notional" live loads coupled with load amplification factors and combined with other maximum state loading conditions (wind, braking, thermal, earthquake, etc.) in combination, is understood to be a largely conservative approach to bridge design. It should also be noted that it is typical for precast segmental post-tensioned concrete bridges, such as these, to be governed by loading conditions during construction, particularly from the balanced cantilever methods of construction and not the in-service loads. Performing physical static load testing of these structures can accurately determine the amount of this reserve capacity.

In 1992, the Average Daily Traffic (ADT) at Kishwaukee Bridge was around 7650 vehicles, but at the beginning of the second millennium, the bridge ADT almost doubled, reaching a value of 14,550 vehicles [37]. With this high increase of ADT, the bridge was subjected to heavier load causing the cracks near the piers to expand. This development prompted the need for an advanced method to assess the shear around the pier. The introduction of the Modified Compression Field Theory and the Strut and Tie modeling represent an advancement in understanding the shear behavior, and both methods are now widely used for concrete shear load rating [38]. Recently, a report published in April 2022 by the FHWA shows the state of practice of the MCFT in shear load rating for bridges. The manual provides different bridge testing and rating example using this method [38].

The rehabilitation phases of I-39 Kishwaukee bridge led to many assumptions if the DLT were to be used. The outcomes of the DLT might not be accurate for higher loads when calibrating the model, especially when the aggregate interlock mechanism is active, and the behavior of the whole bridge might change due to unexpected crack initiation. In addition, the newly installed deviators are transversally anchored to the segments affecting the load distribution across the entire bridge as well as the behavior of the deviator anchorage system with the segment. Also, many segments adjacent to the pier have been subjected to an extensive rehabilitation process, including the implementation of the steel dowels along the shear key and through the web thickness making the simulation of the shear behavior at these regions quite challenging in the model. Moreover, concrete coring reports accomplished before the test shows that the bridge's compressive strength varies significantly from 7500 psi to 12,000 psi in some regions, making it difficult to assign the material properties for the bridge.

This paper illustrates the proof loading test made over the I-39 Kishwaukee River Bridge. It describes the instrumentation plan, testing scenario, and bridge rating results. Also, the study uses the outcomes of the PLT to apply the MCFT to calculate the shear capacity across the cracked section of the bridge. The outcomes of the MCFT can determine if the bridge shear capacity is enough for future load increase and how much is the reserve capacity of the bridge in terms of shear.

3 Instrumentation plan at critical locations for bending and shear

Prior to testing. a finite element analysis on SAP2000 was done by HBM group to determine the critical locations where the highest response is detected for flexural, shear, and displacement. The results show that the highest tensile stresses due to positive moment regions were located at 0.4 L of the bottom flange for the exterior spans. For the interior spans, the highest tensile stresses are at the midspan of the bottom flange. The tensile stresses due to the negative moment peaked at the pier centroid and the two adjacent segments. The FEA also shows that the critical shear stresses were located at the piers and the two adjacent segments. The analysis in the transverse direction showed that the highest critical moment is at the cantilever part of the box girder section. Figures 3, 4 shows the FEA simulation for the maximum positive moment at Span #5 and the maximum shear response at Pier #4, respectively. Figure 5 shows the highest distribution Factor (DF) located approximately 71 ft (0.4 L)

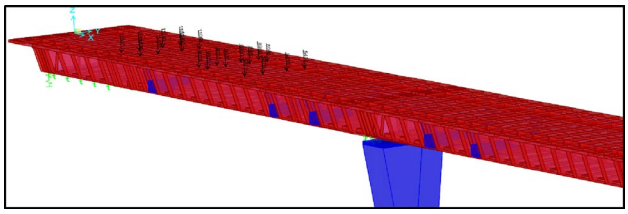

Fig. 3 FEA analysis for the maximum positive moment at Span #5

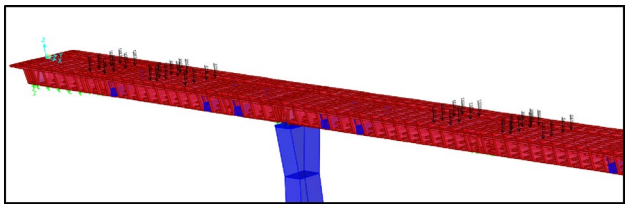

Fig. 4 FEA analysis for the maximum shear response at Pier #4

from the abutment for the bending moment at Span #1. At Piers #4, cracks were greatly visible near the joint. Since a shear failure can cause a sudden collapse of the structure, it is also necessary to investigate the crack opening and the shear stresses during the loading and unloading phase.

Another factor to consider before instrumenting the bridge is the sensor type, model, size, and accuracy to ensure good results with an acceptable error range. The sensor selection depends on the material property, material composition (Homogeneity or heterogeneity), surrounding temperature, humidity, and many other factors. Glisic, in 2011, demonstrated that the accuracy of strain gauges is related to the type of the tested material and strain gauge length. For the structure built with inhomogeneous materials, longer strain gauges are favorable but may feature significant errors in measurement if the strain across the section is non-linear. On the other hand, shorter gauge accuracy is susceptible to errors due to discontinuities (Open cracks). The author demonstrated that when open cracks exist across the section, the strain gauge length should be at least ten times larger than the distance between the cracks L_c [39]. Since the top and bottom flanges of the bridge, as well as parts of the webs, do not show any sign of cracks and discontinuity, hence a Geokon 4000-made model with a gauge length of 150 mm with a ± 0.5% accuracy is used. For the cracked region in the webs, a Geokon displacement transducer model 4420 was used to measure the crack openings during the loading and unloading phase. The model 4420 has a Gauge length of 397 mm and a 12.5 mm reading range with ± 0.1% accuracy. Table 1 shows the sensors model, range, gauge length, and accuracy.

Table 1 Sensor model and specification

Sensor type	Model	Range	Gauge length, mm	Accuracy
Vibrating wire strain gauge	Geokon 4000	3000 με	150	± 0.5%
Displacement transducer, (Crackmeter)	Geokon 4420	12.5 mm	397 mm	± 0.1%

Due to the bridge symmetry, only half of the south-bound bridge was instrumented. Span #3, #4, and #5 were selected for instrumentation at the maximum positive moment, and Pier #4 and #3 were instrumented near the highest shear points and negative moment. Most locations have easy access from inside the box girder cell, and the rest can be accessed from outside. Three different systems were installed on the bridge to study the structure's total behavior: (1) strain gauges to measure the strain in the longitudinal and transversal direction in the concrete, (2) LVDTs to measure

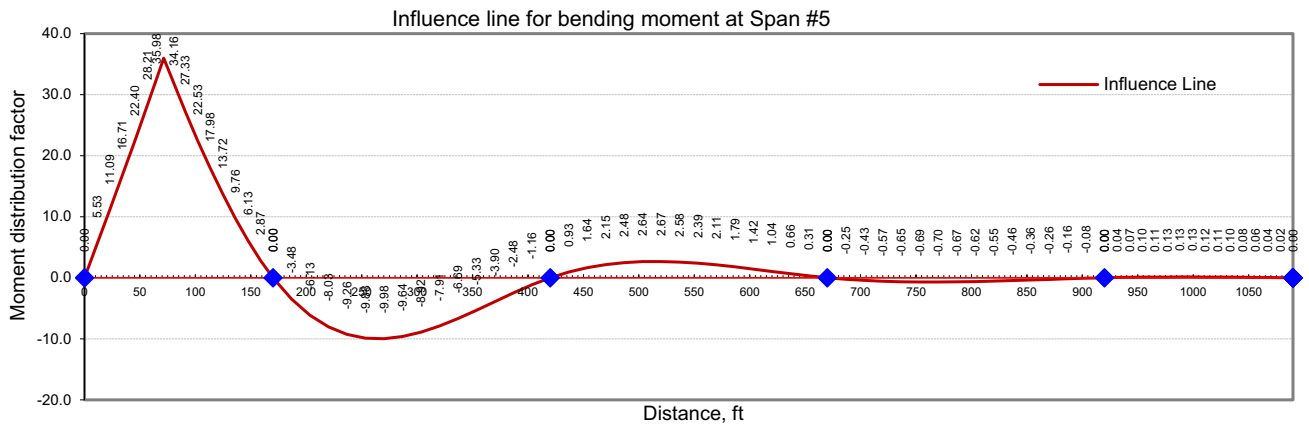

Fig. 5 Influence line for the bending moment of Span #5

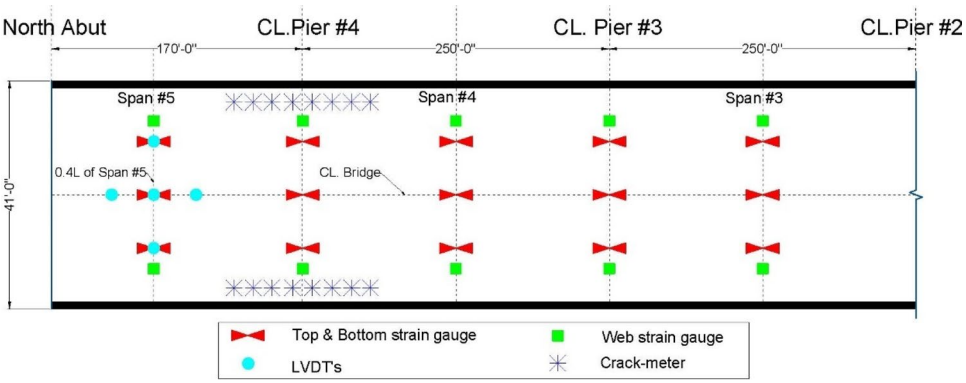

Fig. 6 Plan view of different sensor locations

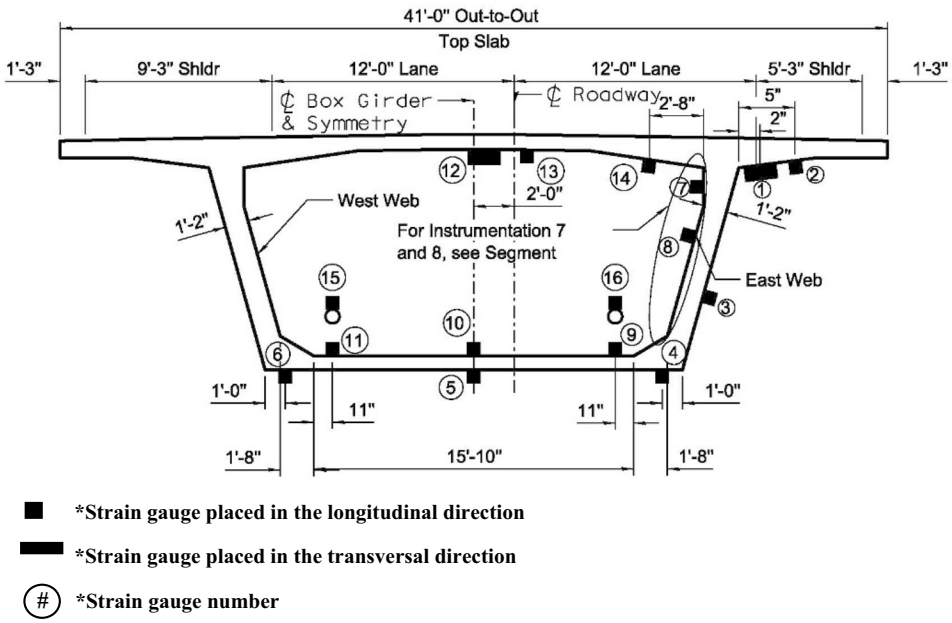

Fig. 7 Strain gauges installed at 0.4 L of Span #5 for the maximum positive moment

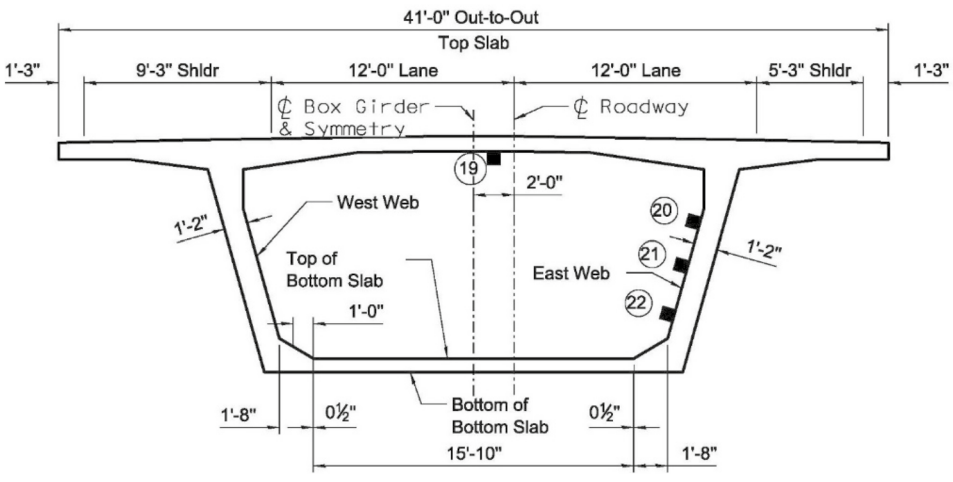

Fig. 8 Strain gauges installed at Pier #4 for maximum negative moment

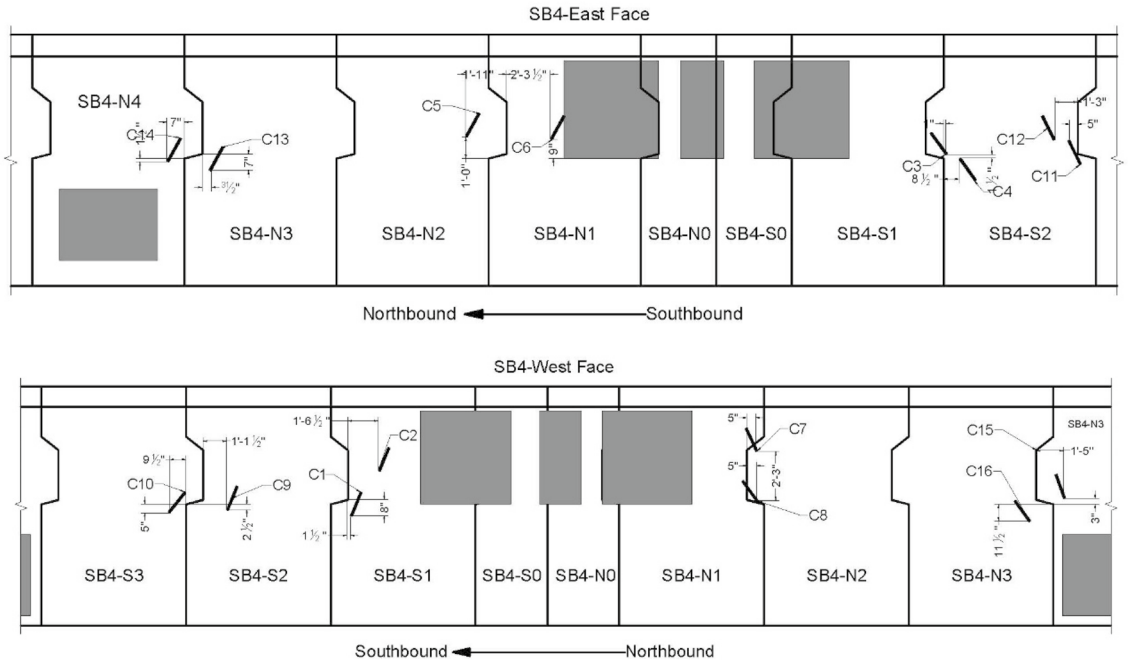

***SB4: South bound, Span #4**
***S#: South bound segment direction**
***N#: North bound direction**
***◝: Crackmeter location**

Fig. 9 Plan of Crackmeter locations

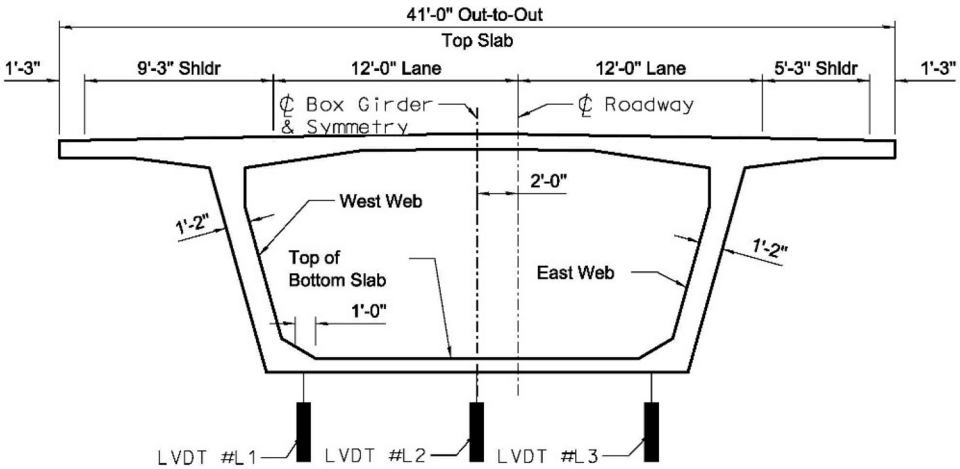

Fig. 10 LVDT typical location plan

the deflection of the bridge, and (3) crackmeters to measure the crack width during the loading test. Sixteen strain gauges were placed at 0.4 lengths (L) of Span #5, eight strain gauges were located at the midspan of Spans #3 and #4, and eight strain gauges were placed for Piers #3 and #4. Figure 6 summarizes the instrumentation plan of the bridge. Figures 7, 8 shows a typical instrumentation section plan for the maximum positive moment located on Span #5 and the maximum negative moment at Pier #4, and the layout of the box girder. The rest of the strain gauge instrumentation section plans are depicted in Appendix Figs. 45, 46, 47, 48, 49, 50, 51, 52, 53, 54. Additionally, sixteen crackmeters were distributed evenly along the webs near Pier #4, as shown in Fig. 9 where most shear cracks and crack propagation are located. Moreover, five LVDTs were installed at 0.4 L of Span #5 to measure the deflection while loading the bridge, as shown in Fig. 10.

Out of 46 strain gauges, 29 were placed on the top and bottom flanges of the box girders to measure the flexural strains in the concrete at the positive and negative

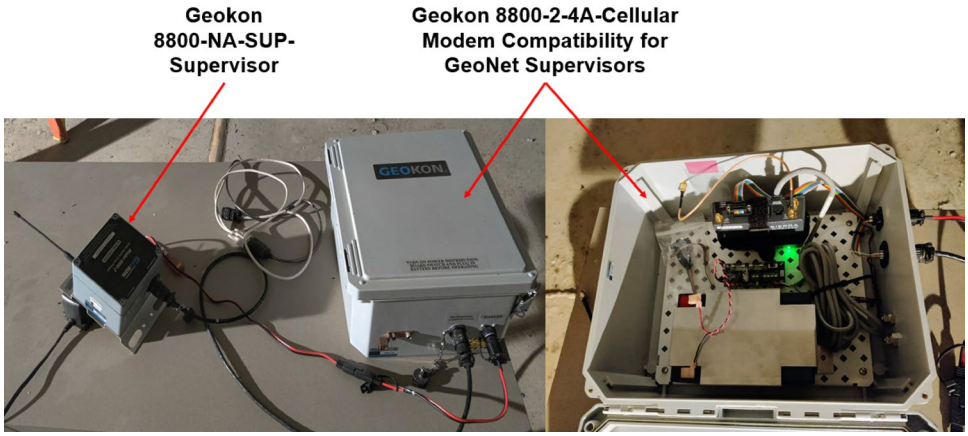

Fig. 11 Geokon supervisor connected to the server modem

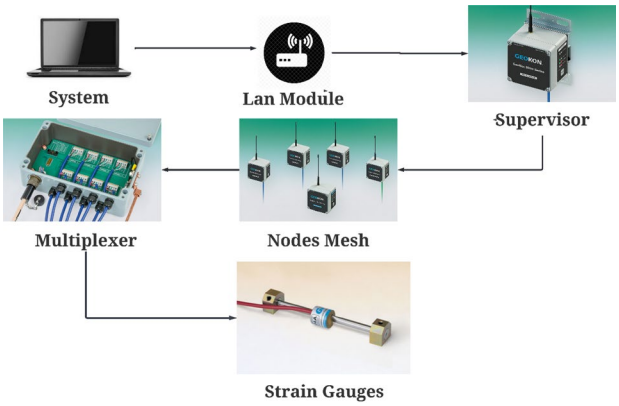

Fig. 12 Flowchart illustrating the hierarchy of the WSN Geokon system

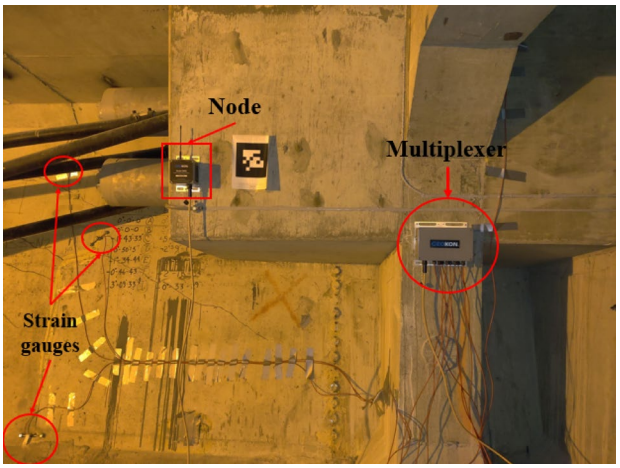

Fig. 13 Instrumented section with strain gauges at Pier #4

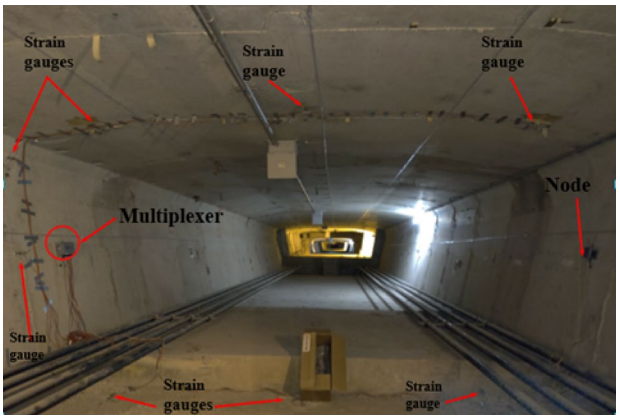

Fig. 14 Instrumented section with strain gauges at mid-span #4

moment region, and two strain gauges were glued on the exterior strands. The east web was instrumented with thirteen strain gauges distributed evenly along each section. Four strain gauge sensors were placed on the web at a 45-degree angle to record the shear strain located between the pier segment and the adjacent segment. The strain gauges used are connected with GeoNet Wireless Network (Geokon) Model 8800 series. The GeoNet system consists of a Mesh Supervisor (Model 8800-NA-SUP-232/USB) and other combinations of single-channel VW Mesh nodes (Model 8800-NA-01C-CBL/10P). Each node is connected to a multiplexer to expand the GeoNet wireless system network's (WSN) capacity to 8 channels. The multiplexer is connected to the node directly with an interconnect cable, and the supervisor is connected to a cellular modem compatible with GeoNet supervisors (Geokon 8800-2-4A) to send the data automatically to the server, as shown in Fig. 11. Geokon Agent software was used for realtime plotting the strain to control the test when any significant decrease in the slope is observed. The flowchart in Fig. 12 summarizes the functioning of the WSN installed at Kishwaukee bridge. Placement details of the strain transducer on the concrete surface for Pier #4 and Span #4 are illustrated in Figs. 13, 14. Figure 15 shows a typical instrumented section with

crackmeters for Pier #4. Sixteen crackmeters are linked to a Geokon 16 channels multiplexer with cables, and the multiplexer is attached to a supervisor. The five LVDTs were placed at critical locations under Span #5 and connected to a five-channel handheld data logger, Tokyo measurement TC-32 k as shown in Fig. 16.

4 Design load vehicles and target-proof load

The main factor during a PLT test is to reach an appropriate live load that is sufficient to encompass any future live load factor, L_T, from vehicles (mainly trucks) and dynamic load allowance without causing permanent damage to the bridge. The AASHTO Manual for Bridge Evaluation [24] states that the bridge rating includes load ratings at the Inventory and Operating levels. It should be noted that for Kishwaukee River Bridges, the shear is the main force that governs the bridge load rating. As the design of the bridges was based on the AASHTO 1979 Standard Specifications, the live design loads consist of the standard AASHTO HS20 tractor-trailer, lane load, or alternate military loading vehicles. The primary HS20 design vehicle is a notational vehicle that consists of a 32.65 Tons (72,000 lb) Gross Vehicle Weight (GVW) tractor/trailer with axle spacings at 4.26 m (14'−0"). The AASHTO Standard Specifications standard group loading combination, including dead load and live load, is abbreviated as:

$$\text{Group(N)} = \gamma \times \left[\beta_{DL} \times D + \beta_{LL} \times (L + I)\right] \quad (1)$$

where γ = Load factor applied to all loads. β_{DL} = Load combination coefficient for dead loads. β_{LL} = Load combination coefficient for live loads. D = Dead load. L = Live load. I = Impact load.

The design vehicle using the AASHTO Load Factor Method consists of a tractor-trailer with a maximum GVW = 205,920 lbs (103 ton) and axle spacings at 14' − 0" centers (excluding impact), resulting in a single axle weight of 91,520 lbs for the Group IA load case as shown in Table 2.

Fig. 15 Crackmeter sensors and system installation at Pier #4

Fig. 16 Portable Data logger TC-32 K connected to LVDTs at bottom of Span #5

Table 2 AASHTO Standards Specifications standard group loading combination

Load Combination	Parameters	The live load (excluding impact)
Group (I)	$\gamma = 1.3, \beta_{LL} = 1.67, \beta_{DL} = 1$	70Tons + IM (156,240 lb + IM)
Group (IA)	$\gamma = 1.3, \beta_{LL} = 2.20, \beta_{DL} = 1$	93Tons + IM (205,920 lb + IM)

Table 3 Type I vehicle weight and axle spacing diagram

Type I-vehicle data-38 Tons				Type I-vehicle data-45 Tons			
Axle	Weight tons (lbs)	Vehicle dimensions in m (ft)		Axle	Weight tons (lbs)	Vehicle dimensions in m (ft)	
–	–	A	6.01 (19.75)	–	–	A	6.01 (19.75)
1	4.85 (10,700)	B	1.37 (4.50)	1	5.81 (12,811)	B	1.37 (4.50)
2	8.01 (17,670)	C	9.52 (31.25)	2	9.59 (21,157)	C	9.52 (31.25)
3	8.01 (17,670)	D	3.1 (10.17)	3	9.59 (21,157)	D	3.1 (10.17)
4	8.50 (18,740)	E	11.12 (36.50)	4	10.17 (22,438)	E	11.12 (36.50)
5	8.50 (18,740)	F	8.88 (29.17)	5	10.17 (22,438)	F	8.88 (29.17)
Total	GVW = 38 (82,000)	$E+F$ = 20 m (65.67)			GVW = 45 (100,000)	$E+F$ = 20 (65.67)	

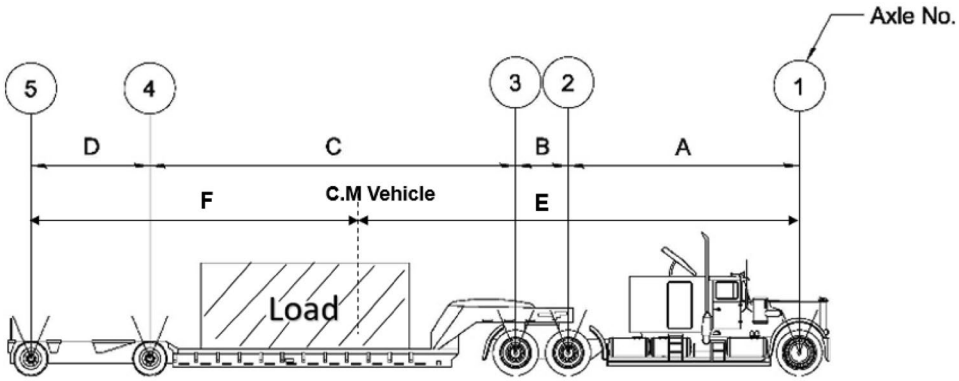

The current maximum legal weight allowed by the Illinois Department of Transportation (IDOT) on a single axle Special Haul Vehicle is 20,000 lbs which is approximately 20% of that for which the bridge was designed. The type I vehicles, as shown in Table 3, consisted of tandem axle tractors and tandem axle trailers loaded with crane counterweight boxes and hoisting equipment weighing approximately 38 and 45 tons for the first two load increments, respectively. The Type II vehicles, as shown in Table 4, consisted of tri-axle tandem tractors with tri-axle tandem low-boy trailers and carried a single 36-ton locomotive crane equipped with a counterweight as payload weighing approximately 61 and 68 tons for the 3rd and final loading increments, respectively. The maximum truck weight selected is 68 tons, and when analyzed, this vehicle produced demands less than the unfactored 72,000 lb (32.65 tons) AASHTO HS20-44 design vehicle, which provided a comfortable margin of safety against overloading the structure during testing.

5 Experimental program and operation

A detailed load testing procedure is conducted to apply the target proof load L_T (75 Tons) in stages. Based on the MBE [24] the first and second loading stage should not exceed 0.25 L_T and 0.5 $0L_T$ respectively. After that, small increments of loading can be used, especially when the applied load draws near the maximum calculated truck loading L_T[24]. Due to the high traffic volume on route I-39, roughly 16,300 vehicles per day, it is not reasonable or economical to completely close a major interstate for long periods. Therefore, four load increments were selected to reduce the number of overall tests required to be performed. The experimental program aims to test the bridge in 9 positions to adequately envelope the bridge behavior. Table 5 shows the positions and the type of test made on the bridge during the rating.

Maintenance of traffic was provided by the Illinois Department of Transportation (IDOT). A moving lane closure with signal trucks and traffic attenuators was deployed to reduce the highway traffic speed and allow for a 20-min window where the bridges were free from traffic. Before testing, all truck positions were mapped out and optimized to allow for the maximum number of tests during a single closure. The logistical constraints of quickly mobilizing successive load increments required close coordination with the maintenance of traffic personnel and the test vehicle drivers. The testing was broken up into three separate nights, as described in Table 6. The four load increments used for testing were separated into two vehicles, "Types", Type 1, and TypeII, each with two load increments as shown in Figs. 17, 18, 19, 20. The testing was broken up into three separate nights, and during each position, the trucks were stopped for 5 min to ensure that the amount of data collected during this interval was consistent.

Table 4 Type II vehicle weight and axle spacing diagram

Type II-Vehicle Data-61 Tons				Type II-Vehicle Data-68 Tons			
Axle	Weight Tons (lbs)	Vehicle Dimensions in m (ft)		Axle	Weight Tons (lbs)	Vehicle Dimensions in m (ft)	
–	–	A	4.42 (14.50)	–	–	A	4.42 (14.50)
1	4.79 (10,560)	B	1.45 (4.75)	1	5.10 (11,260)	B	1.45 (4.75)
2	9.00 (19,850)	C	1.37 (4.50)	2	10.11 (22,300)	C	1.37 (4.50)
3	9.00 (19,850)	D	10.75 (35.25)	3	10.11 (22,300)	D	10.75 (35.25)
4	9.00 (19,850)	E	1.37 (4.50)	4	10.11 (22,300)	E	1.37 (4.50)
5	7.25 (16,000)	F	1.37 (4.50)	5	8.16 (18,000)	F	1.37 (4.50)
6	7.25 (16,000)	G	1.37 (4.50)	6	8.16 (18,000)	G	1.37 (4.50)
7	7.25 (16,000)	H	12.11 (39.74)	7	8.16 (18,000)	H	12.11 (39.74)
8	7.25 (16,000)	I	9.98 (32.76)	8	8.16 (18,000)	I	9.98 (32.76)
Total	GVW= 61 (134,000)	H+I=22.10 (72.50)			GVW= 68 (150,000)	H+I=22.10 (72.50)	

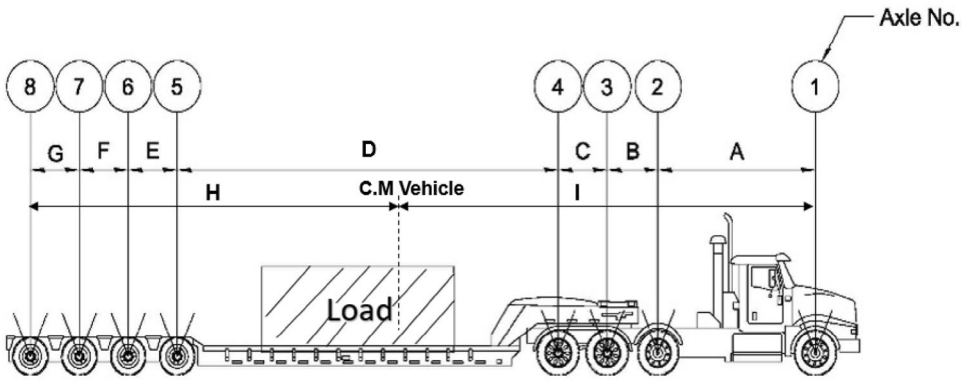

Table 5 Testing locations and objectives

Position #	Test objectives
Position #1	Maximum flexure in Span 5 Maximum positive moment at 0.4L of Span #5 Maximum top slab transverse positive flexure at the centerline of the bridge
Position #2	Maximum negative moment at Pier #4
Position #3	Maximum negative moment Pier #3
Position #4	Maximum positive moment at midspan of Span #4
Position #5	Maximum positive moment at 0.5 L of Span #3
Position #6	Maximum negative transverse flexure at the cantilever wing
Position #7	Maximum negative transverse flexure at the centerline of top slab
Position #8	Maximum combined shear and torsion to the south of Pier #4
Position #9	Maximum combined shear and torsion to the south of Pier #3

Table 6 Testing schedule

Night	Type/ # of vehicles	Test load
1	Type I/4 vehicles	38 and 45 Ton (82,000 and 110,000 lbs)
2	Type II/4 vehicles	61 Ton (134,000 lbs)
3	Type II/2 vehicles	68 Ton (150,000 lbs)

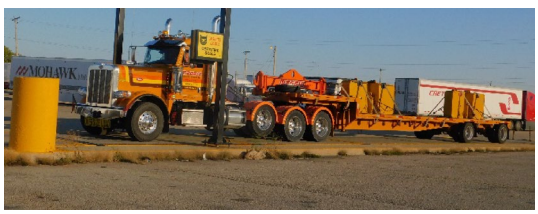

Fig. 17 Type I Test vehicle loaded with counterweights, 38 Tons test

Fig. 18 Type I Test vehicle loaded with counterweights, 45 Tons test

Fig. 19 Type II Test vehicle loaded with crane, 61 Tons test

Fig. 20 Type II Test vehicle loaded with crane and counterweight, 68 Tons test

The proof load test was accomplished in three consecutive nights between 8 PM and 2 AM. Both lanes of I-39 Kishwaukee bridge were closed to traffic for approximately one mile beyond each end of testing bridge.

5.1 Test itinerary and truck position

Figure 21 shows the testing itinerary used in the field and the vehicle positions during each load test. A plan view, side view, and an aerial view for a typical maximum negative moment at Pier #3 is shown in Figs. 22, 23, 24, respectively.

6 Observed linear elastic behavior for strain gauges readings

Linear elastic behavior was observed. The moment versus strain resulting from the load applied was plotted in terms of increasing the test load and peak strain measurement reading from all the sensors. Based on the sensor locations, strain responses for the maximum positive and negative moment, maximum shear, and maximum torsion effect were plotted. The longitudinal strain gauges are represented by the letter "L" and the transversal ones are represented by the letter "T", followed by the number depicted in the instrumentation plans (Figs. 25, 26, 27, 28,

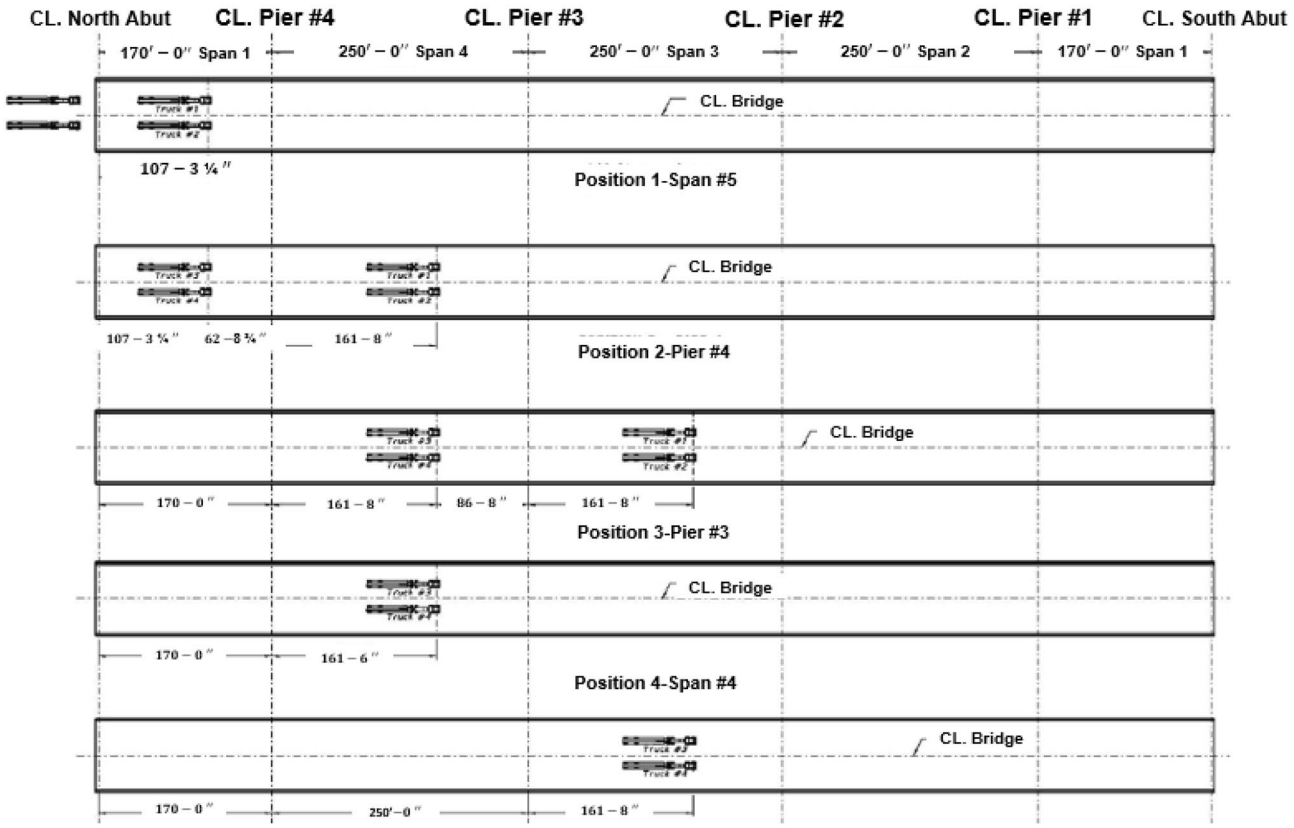

Fig. 21 Testing Positions

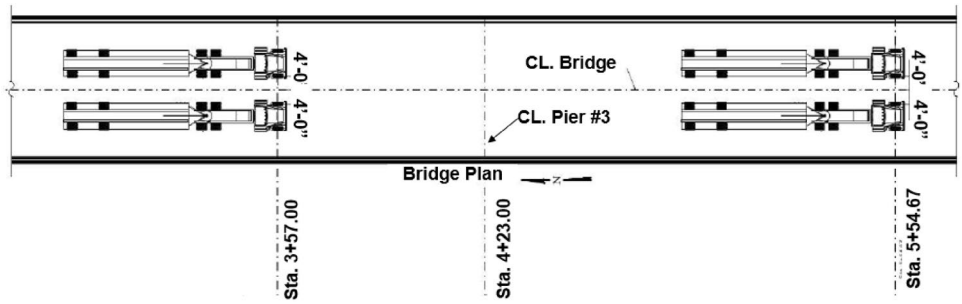

Fig. 22 Top view of bridge for maximum negative moment at Pier #3

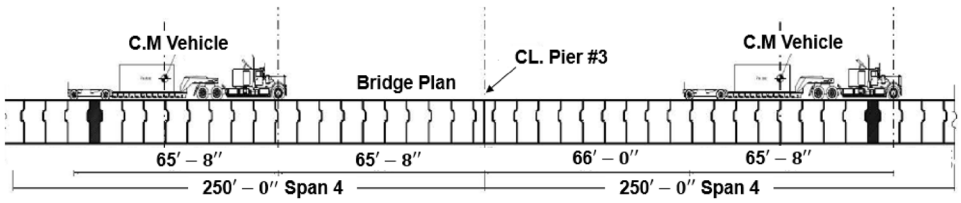

Fig. 23 Elevation view of the bridge for the maximum negative moment at Pier #3

Fig. 24 Aerial view of the bridge for the maximum negative moment at Pier #3

29, 30). For a linear elastic behavior, it should be noted that the strain curves are expected to be linear when the load increase. The linearity represents the stiffness of the bridge in terms of moment increase (load increase) relative to the strain increase. During proof loading, an apprehensive control should be considered when any significant slope decrease is observed during load increase. This indicates that the bridge at this location is losing stiffness, and non-linear behavior is observed caused by particular distress or cracks development [5]. A non-linear behavior is observed when several slopes start to decrease and worsen whenever the load increases signaling the end of the test to protect the bridge from any permanent damage. GEOKON Agent software corrects the temperature effect on the strain reading for each gauge using the formula below:

$$\text{Microstrain } (\mu\varepsilon) = \left(R_1 - R_0\right)GF + \left(T_1 - T_0\right)K \tag{2}$$

where R_1 = current reading position, R_0 = initial reading, T_1 = current temperature in °C, T_0 = initial temperature in °C, K = 12.0 microstrain/°C

For Spans #5, #4, and #3, the moment versus peak strain curves are presented in Figs. 25, 26, 27, respectively. At the moment versus strain response plot, the slope of the line for each strain gauge is almost linear and doesn't change when the load increment is increased. For the maximum negative moment at Pier #4, the moment versus peak strain curves

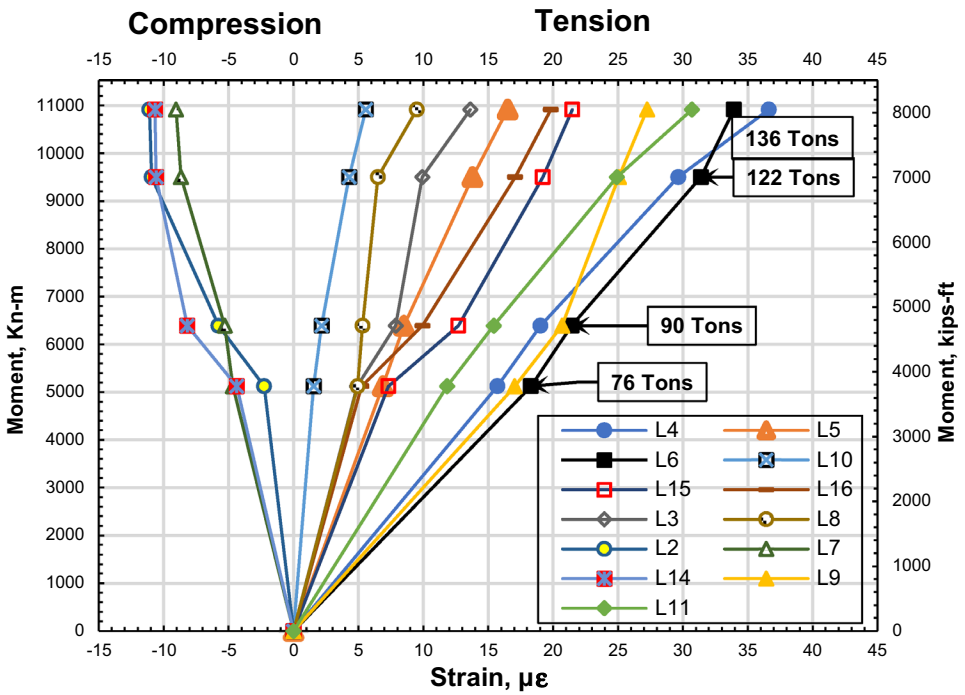

Fig. 25 Moment-strain in compression and tension at 0.40L of Span #5

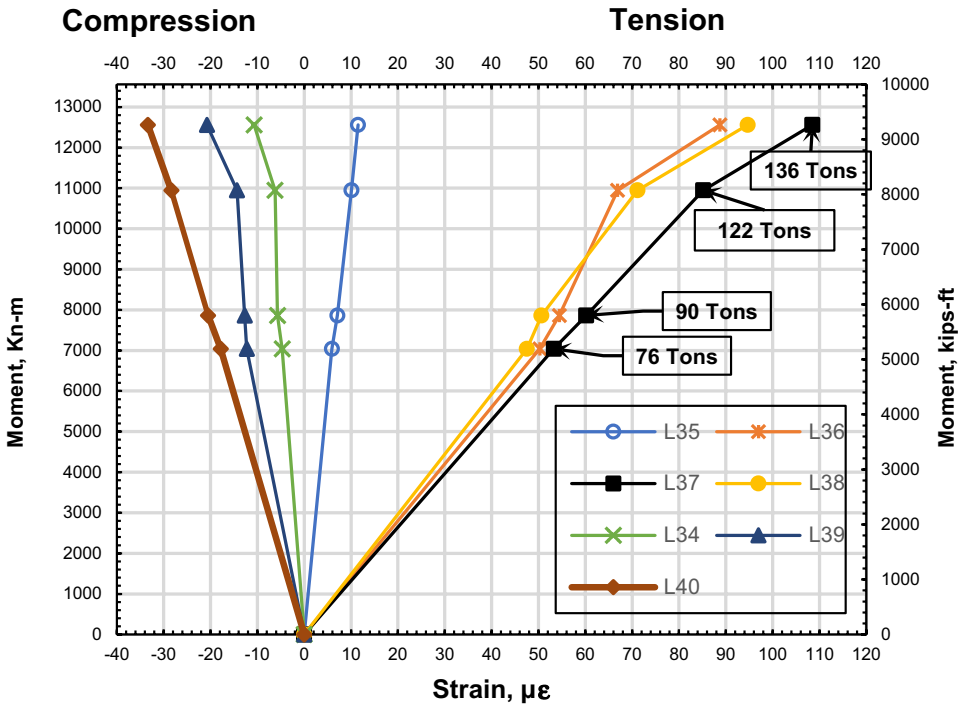

Fig. 26 Moment-peak strain in compression and tension at midspan #4

are shown in Figs. 28, 29, and all the strain gauges show a perfect linear behavior. The same results were observed for Pier #3 in Fig. 30. Transverse strains T1 and T12 exhibited a linear behavior with a maximum recorded compressive strain of 56 με at T1, as shown in Fig. 61. The data for the rest of the strain gauges are illustrated in the Appendix Fig. 55, 56, 57, 58, 59, 60, 61, 62, 63, 64.

Figure 31 shows the strain readings over the height of the girder and how the neutral axis height is shifting upward when the live load increase for Span #3.

The highest strain recorded from the maximum truck loading of 136 Tons is 113$\mu\varepsilon$ at strain gauge L46 located at the bottom flange of Midspan #3 as shown in Fig. 32.

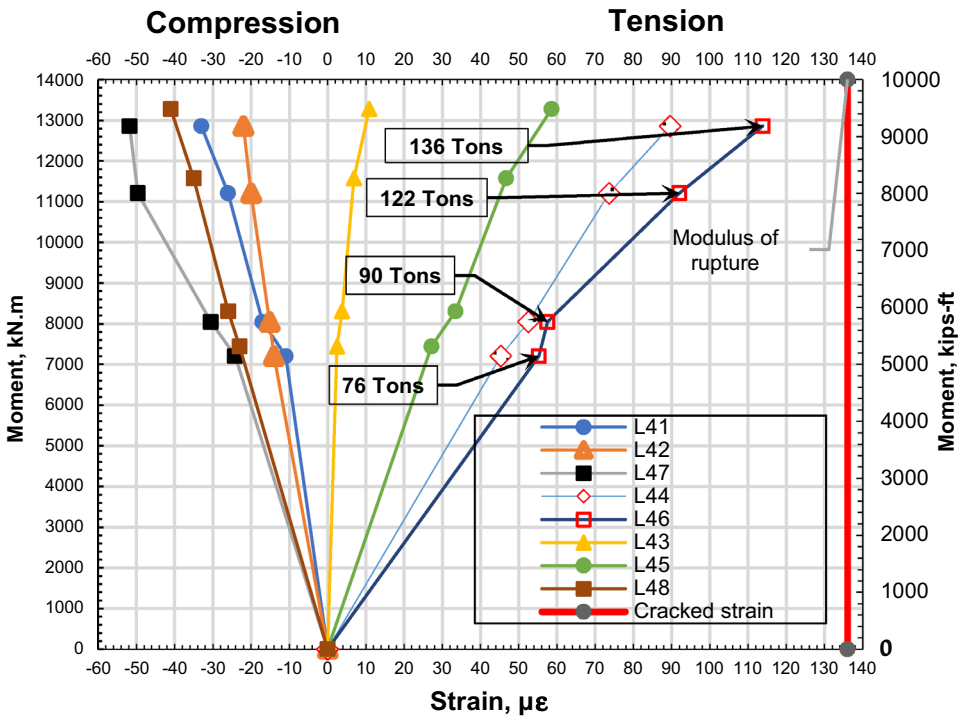

Fig. 27 Moment-peak strain curves in compression and tension at Midspan #3

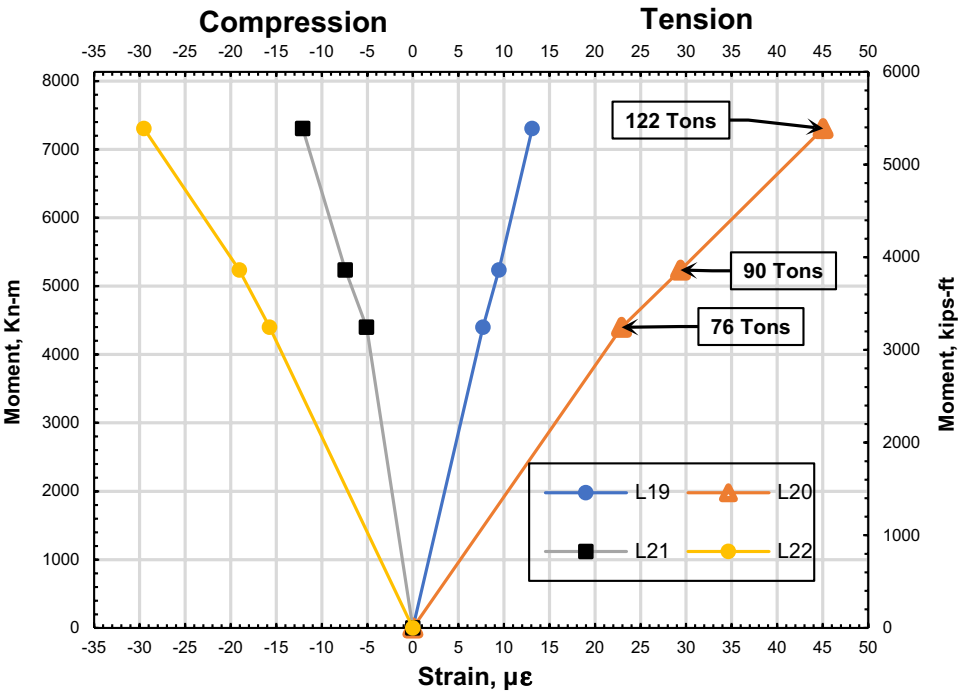

Fig. 28 Moment-peak strain curves in compression and tension at Pier #4 SB4-S2 section

The compressive strength of Kishwaukee bridge tested on site is $f_c^{'} = 51.70$ MPa (7500 psi).

From AASHTO LRFD C5.4.2.4–2 [40] the modulus of elasticity is giving by:

$$E_c = 33,000\ k_1 w_c^{1.5} \sqrt{f_c'} \tag{3}$$

where k_1 = Correction factor for source of aggregate to be taken as 1.

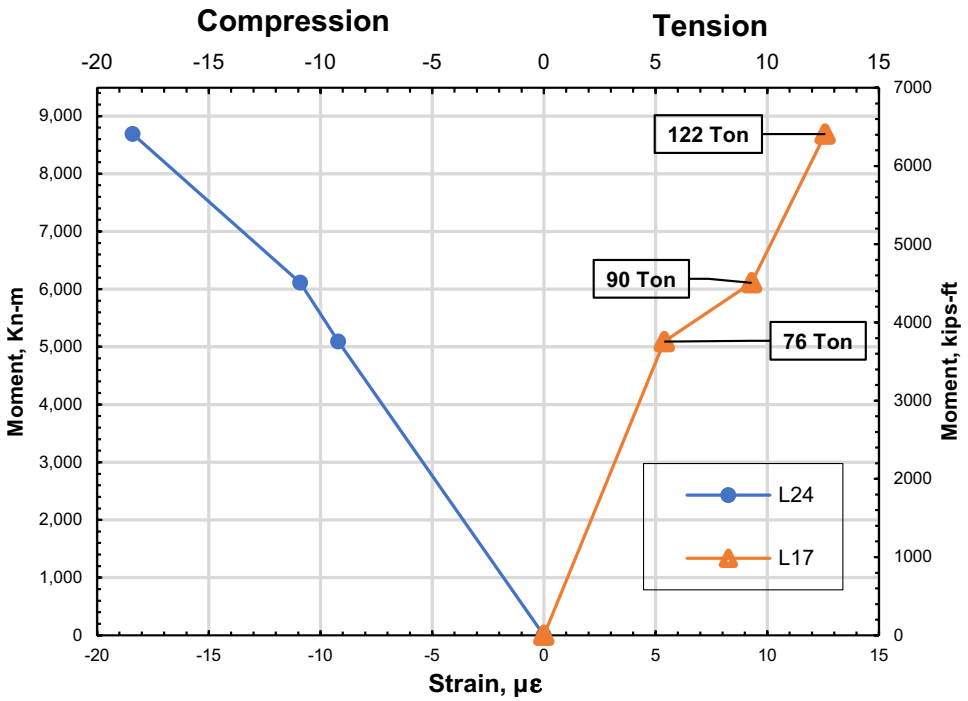

Fig. 29 Moment-strain curves in compression and tension at Pier #4 SB4-S2 section

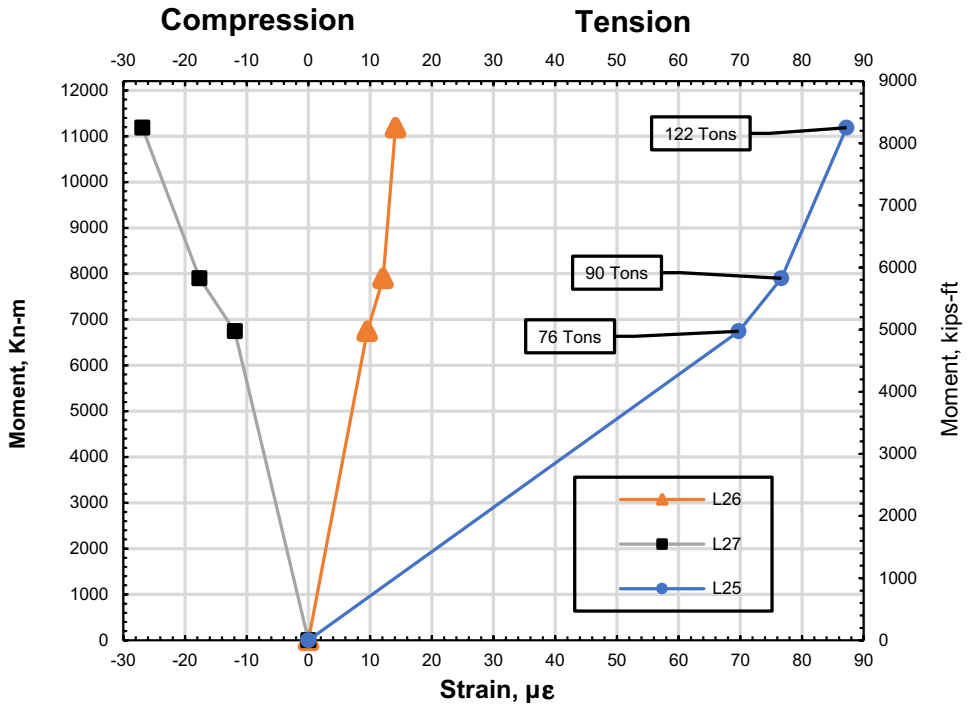

Fig. 30 Moment versus peak strain curves in compression and tension at Pier #3, SB3-N1 section

$w_c = 145 lb/ft^3 (2322 kg/m^3)$

$E_c = 4{,}989{,}954$ psi(34404.49 MPa)

Having an elastic modulus of $E_c = 4{,}989{,}954$ psi, the modulus of rupture f_r given from AASHTO LRFD 5.4.2.6 is:

$$f_r = 0.24 \times \sqrt{7.5} = 657 \text{ psi } (4.52 \text{ Mpa}) \quad (4)$$

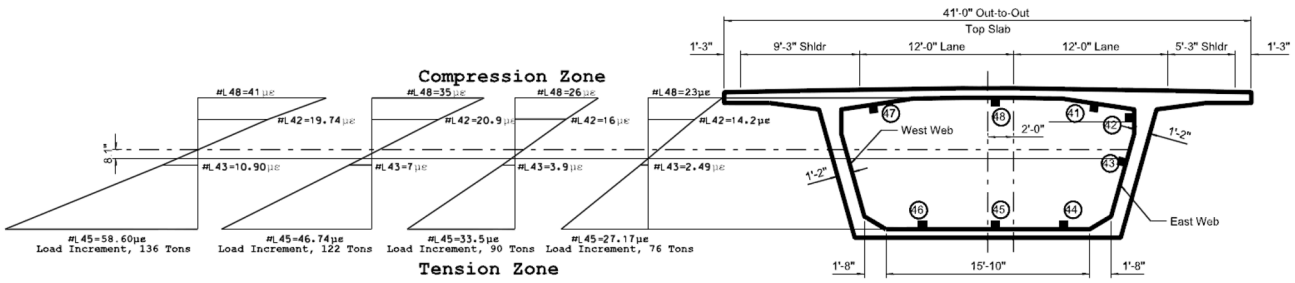

Fig. 31 Compression-Tension strain diagram variation under loading at Span #3

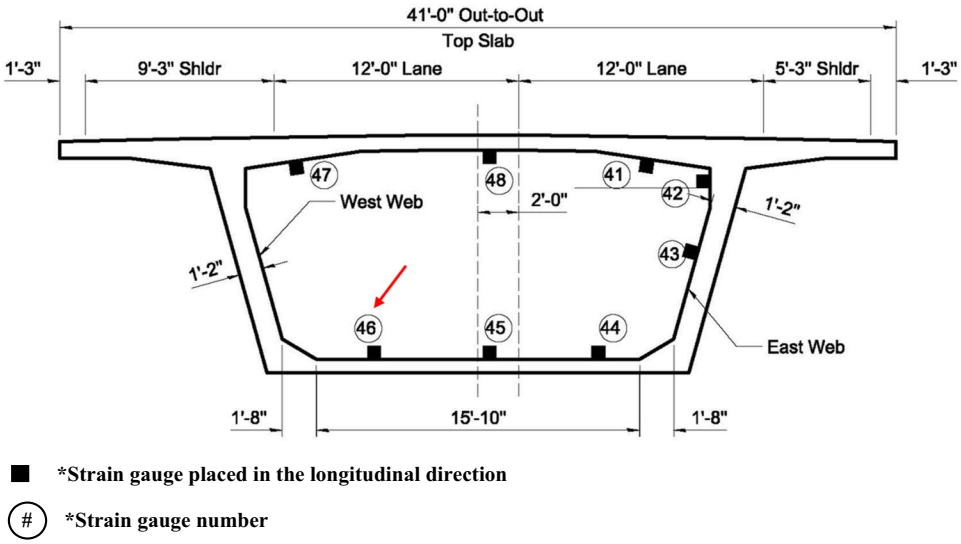

Fig. 32 Strain gauges at Midspan #3 for the maximum positive moment

The total stress generated at this location is:

$$\sigma = E_c \times \varepsilon = 563 \text{ psi} < 657 \text{ psi } (3.88 \text{ Mpa} < 4.52 \text{ Mpa}). \quad (5)$$

The recorded flexural stress is less than the modulus of rupture, indicating that the concrete did not reach the cracking point. The validation of the linear elastic behavior of the bridge also requires that all strain gauges return to their original calibrated strain value once the load is removed. The strain gauges for all the test runs returned to zero after unloading, and no residual strain was observed; this concludes that the bridge is still behaving in the elastic range, and no distress is observed.

Fig. 33 Crack width initial reading measurement

Kishwaukee bridge is governed mainly by the shear stresses located near the Piers. During Positions #2 and #8, sixteen crackmeters distributed along Pier #4 recorded the crack growth on each loading stage. Each crack width was measured at rest when no loading was acting on the bridge, as shown in Fig. 33. Figures 34, 35, 36, 37 depict the crack growth for the crackmeters (C1–C16) at Position #8. Although strain gauges demonstrated that the tested bridge behaved linearly, crack width recording is more complicated, and unlike the strain gauges, crack behavior doesn't have to depict always a linear behavior due to many factors such as (1) the existence of neighboring cracks along the same crackmeter, (2) aggregate interlock effect, and (3) temperature. Most importantly, all crack openings were checked after each loading stage, and all the sensors recorded the original measured width meaning

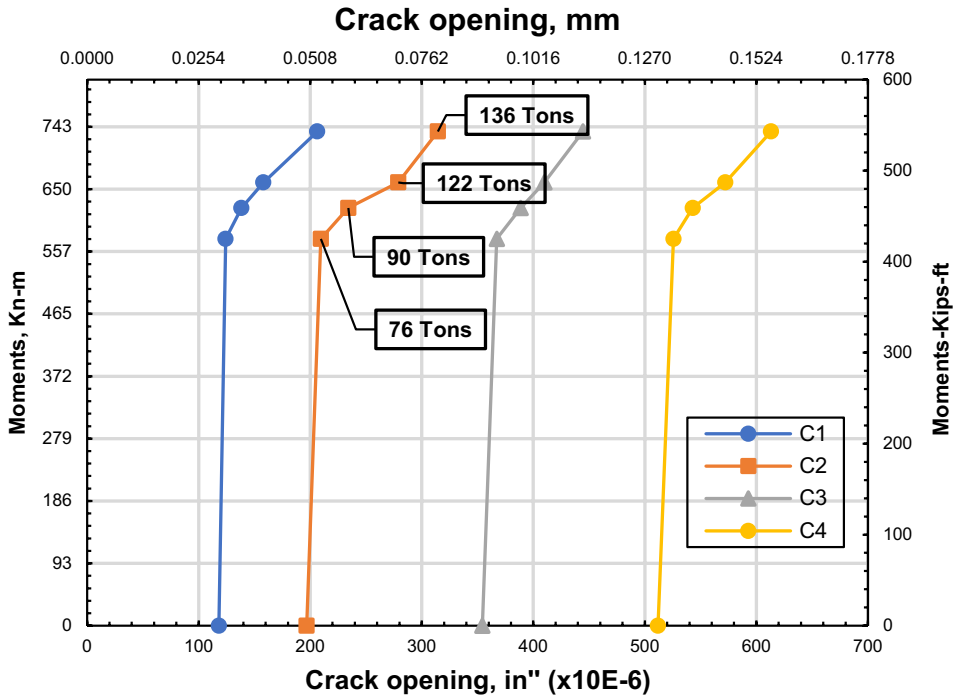

Fig. 34 Crackmeter readings at Pier #4, Section SB4-S1/ NB4-S1

that after the loading and unloading phases, the bridge returned to its original state and proved to be elastic.

The next stage is to measure the deflection at 0.40L of Span #5 when the truck loading is at Positions #1 and Position #6. Figures 38, 39, 40 shows the load–deflection curves at 0.40L of Span #5. The five LVDTs showed perfect linear behavior and returned to their original reading values with no residual deflection observed. For Position #6 shown in Fig. 41, the torsion behavior was perfectly translated when a 71 Tons truck was placed on one side of the bridge, above the LVDT #L1. The deflection curves in Fig. 42 show a maximum value of 2.28 mm of displacement at L1 and decreased linearly to reach a minimum value of 1.30 mm on L3, resulting in 0.98 mm of uplifting over a total width of 6 m. This difference Exhibited negligible torsional effect. LVDT #L1 measured a maximum deflection of 4 mm at Position #1 under a total live load of 136 tons. Based on AASHTO LRFD clause 2.5.2.6.2, the maximum allowable deflection criteria under vehicular load, including the Impact Factor (IM) and presence factor (m) is given from the following equation:

$$\begin{aligned} &\textit{Maximum recorded deflection} \\ &< \textit{Maximum allowable live load deflection} 0.004 \text{ m} \\ &< \frac{\text{Span Length}}{800} = \frac{51.81 \text{ m (170 ft)}}{800} \end{aligned} \tag{6}$$

$$0.004 \text{ m} < 0.064 \text{ m}$$

Equation 6 shows that the maximum deflection of Span #5 measured under a live load of 136 tons is 6.2% of the maximum allowable deflection. The deflection results demonstrated that the I39-Kishwaukee bridge is stiff and stable.

7 Bridge load rating results

AASHTO MBE Sect. 6A.5.11.4 specifies that under inventory rating analysis, the strength and service cases shall be checked for the design live load (HS20-44) utilizing the number of design lanes (3 Lanes) [24]. At the Operating level analysis, the number of stripped lanes (2 lanes) can be considered and positioned transversely to create the maximum effect when rating at the service level. Strength conditions at the Operating level must still use the number of design lanes. Kishwaukee River Bridge was constructed prior to October 2010, so the Load Factor Method (LFD) and Allowable Stress Method (ASM) are applied. Capacities, resistance factors, and distribution factors are based on AASHTO Standard Specifications, 17th edition. Table 7 presents the bridge rating summary for allowable stresses needed.

The Rating equation is given from AASHTO MBE Eq. 6B.4.1–1 [24].

$$\text{RF} = \frac{C - A_1 D}{A_2 L(1 + I)} \tag{7}$$

where: RF = Rating factor, C = Nominal member resistance, D = Unfactored dead loads, L = Unfactored live

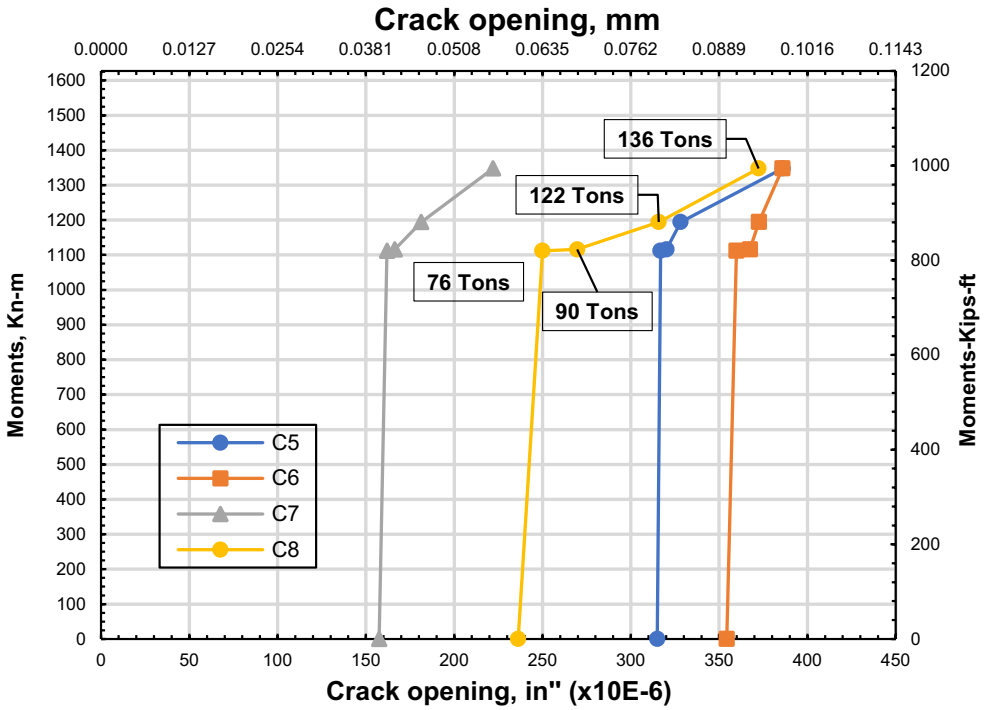

Fig. 35 Crackmeter readings at Pier #4, Section SB4-N1/NB4-N1

Fig. 36 Crackmeter readings at Pier #4, Section SB4-S2/NB4-S2

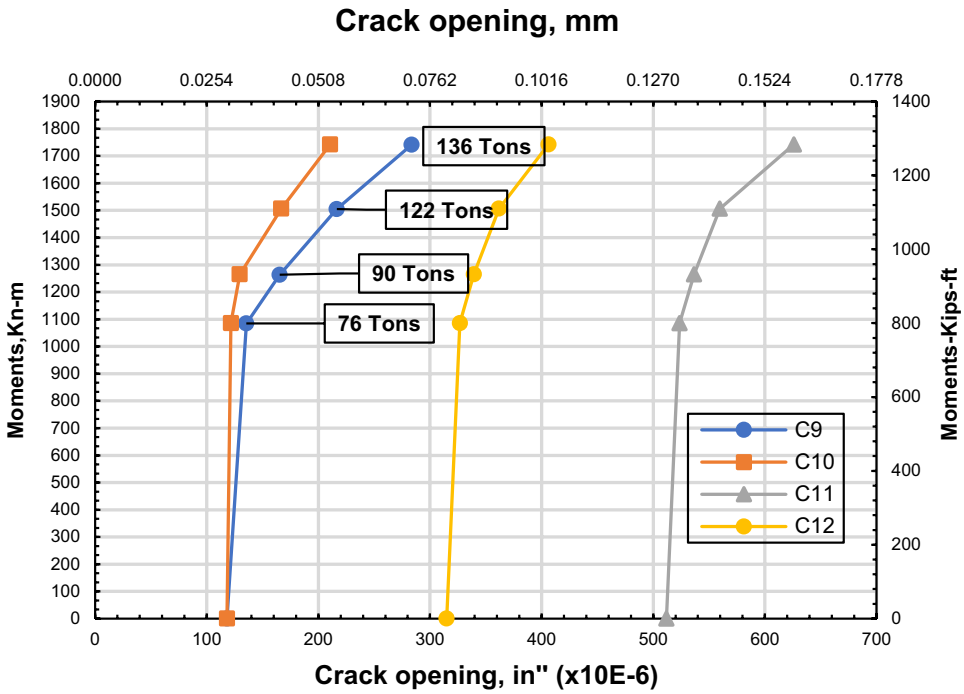

loads, I = Impact factor to be used with the live load effect, A_1 = Dead load factor depending on the rating level desired, as shown in Table 8. A_2 = Live load factor depending on the rating level desired, as shown in Table 8.

For segmental bridges, the bridge rating is made for each segment and not just on the bridge critical locations. Based on Tables 9 and 10, the following equations were utilized at each respective level of rating.

Given the PLT values for the live load extracted under different positions and loading increments, the highest live load increment is considered for rating the Kishwaukee I-39 bridge. For each bridge segment, all the required dead loads

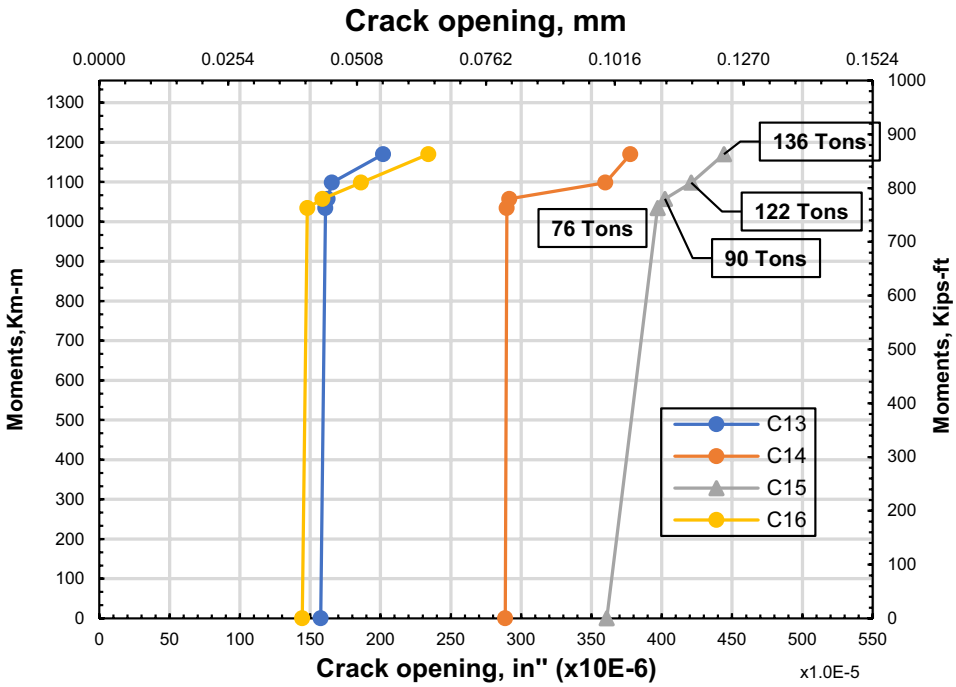

Fig. 37 Crackmeter readings at Pier #4, Section SB4-N3/ NB4-N3

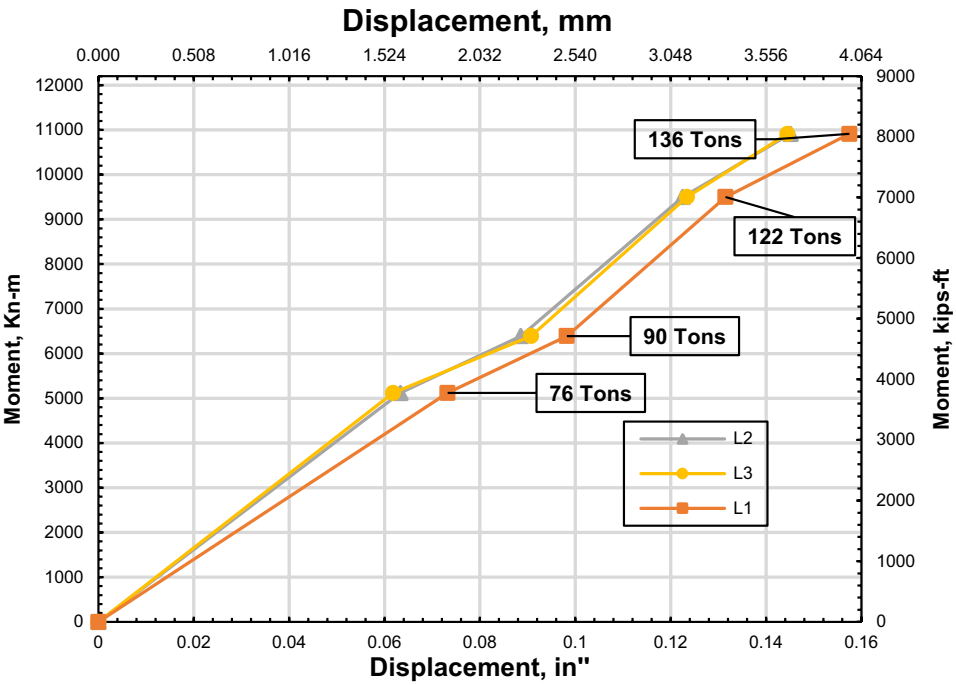

Fig. 38 Moment-deflection curves located at 0.40L of Span #5

(stresses, shear, and moment) were calculated, and the live load's stresses were derived from the highest truck loading increment. The controlled rating factor is selected from the bridge segment with the smallest rating factor for each rating scenario. Tables 11 and 12 summarize the calculated rating factor at each scenario for the inventory and operating levels, respectively.

As indicated in Tables 11 and 12, all the Rating Factors are greater than 1. It can be noticed that the controlling Inventory and Operating Rating Factor are 1.21 and 1.59,

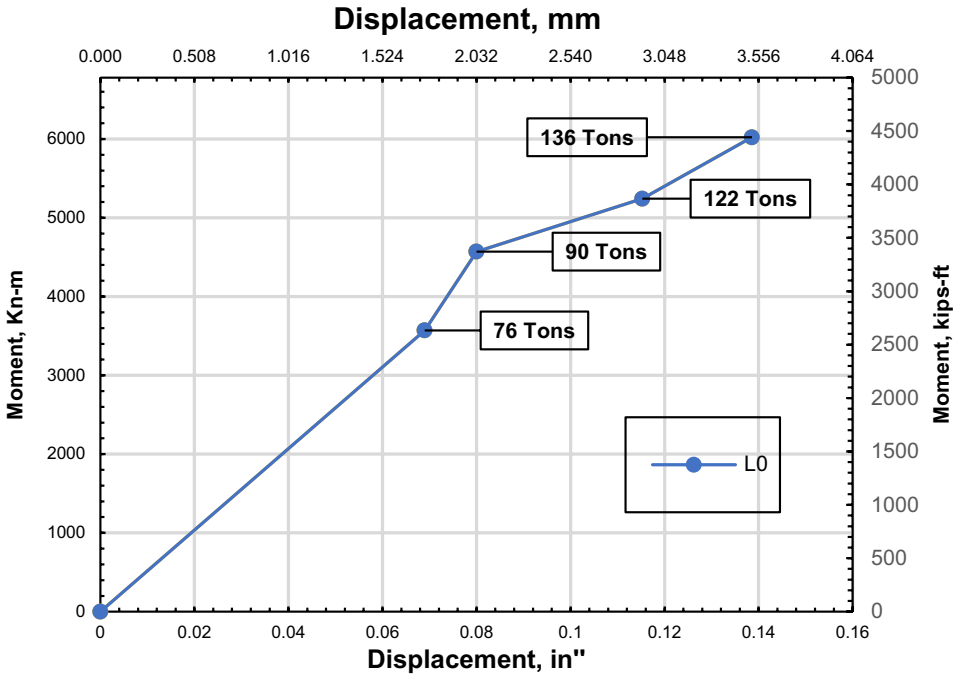

Fig. 39 Moment-deflection curves located at Span #5, Section SB5-S5A

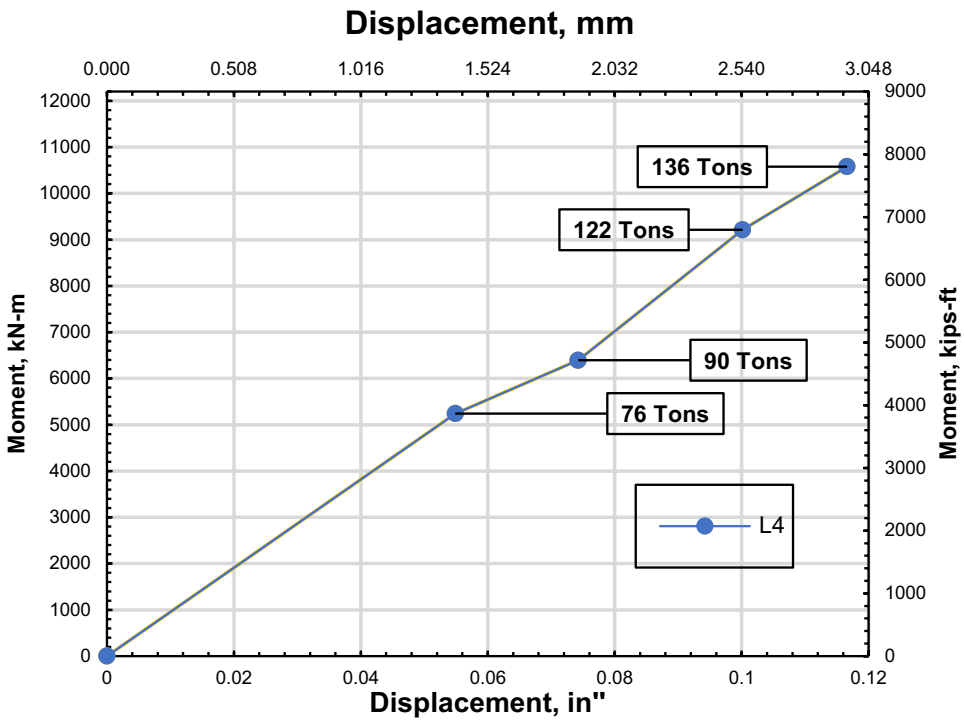

Fig. 40 Moment-deflection curves located at Span #5, Section SB4-N11A

respectively, obtained from the transverse top slab tensile stresses condition. Based on the proof load test results discussed above, the bridge was physically and analytically proven safe.

8 Shear assessment using the modified compression field theory

Initially, the Compression Field Theory assumed that once web cracking occurs, the principal tensile stress

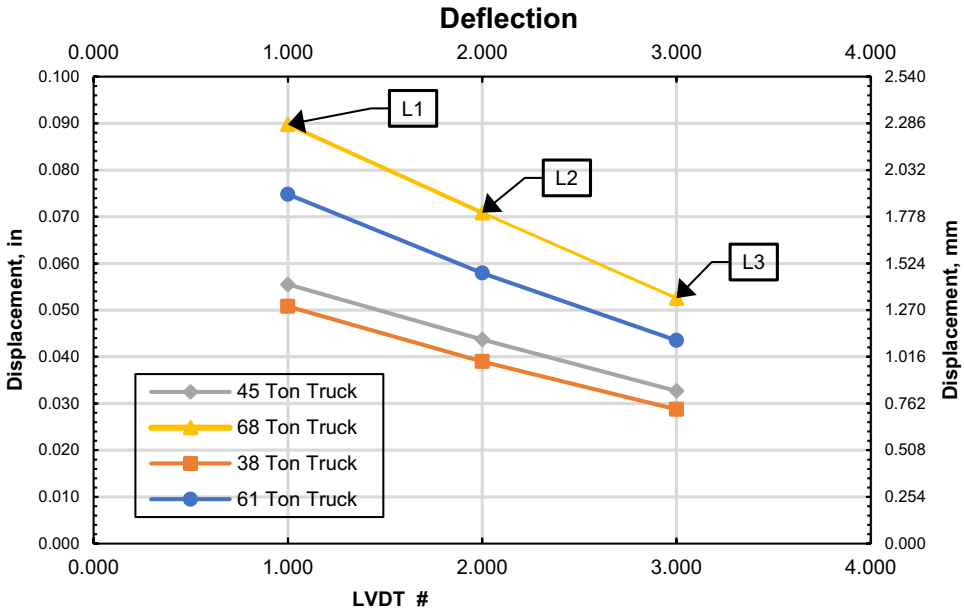

Fig. 41 LVDT behavior due to torsion at Position #6 for different loading increments

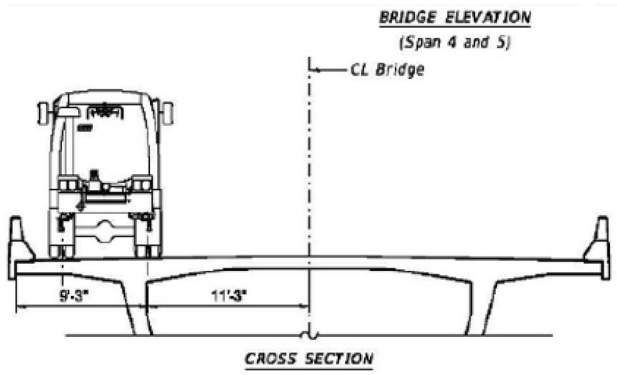

Fig. 42 Truck loading for Position #6

Table 8 Dead and live load factor

Load factor	Allowable stress design (ASD)		Load factor design (LFD)	
	Inventory level	Operating level	Inventory level	Operating level
Dead load factor A_1	1	1	1	1
Live load factor A_2	1	1	2.17	1.3

vanishes. After cracking, the tensile stresses across the crack are carried by the web reinforcement, and the concrete strut carries the compressive stresses. As a result, the conventional Mohr's circle is not applicable, and the orientation of the principal stresses changes to an angle θ of less than 45° [41].

8.1 Aggregate interlock mechanism

In principles, the modified compression field theory is used to estimate the ability of cracked concrete to carry shear as

Table 7 Summary of allowable stresses

Service level after losses	Stress limit, C (inventory rating)	Stress limit, C (operating rating)	Source of criteria
Long. tension	0 psi (No tension, 3 Lanes loaded)	0 psi (No tension, 2 Lanes loaded)	AASHTO GSSB Sec. 9.2.2.2
Trans. tension	$3\sqrt{f'_c}$ (3 Lanes Loaded)	$6\sqrt{f'_c}$ (2 Lanes Loaded)	AASHTO Std. Specs, Sec. 9.15.2.2
Compression 1 (Long or Trans	$0.6\ f'_c$ (3 Lanes Loaded)	$0.6\ f'_c$ (2 Lanes Loaded)	AASHTO Std. Specs, Sec. 9.15.2.2 AASHTO MBE., Sec. 6B.5.3.3
Compression 2 (Long or Trans)	$0.4\ f'_c$ (3 Lanes Loaded)	$0.4\ f'_c$ (2 Lanes Loaded)	AASHTO Std. Specs, Sec. 9.15.2.2 AASHTO MBE., Sec. 6B.5.3.3

*Long = longitudinal

*Trans = transversal

Table 9 Inventory level analysis rating cases

Rating equation	Service Level (ASD)
$RF = \frac{0-[f_{d1}-f_{d2}-f_{p1}-f_{p2}-f_{EL}-f_s-f_{cs}]}{f_l}$	Long. concrete tensile stress
$RF = \frac{0.6f'_c-[f_{d1}-f_{d2}-f_{p1}-f_{p2}-f_{EL}-f_s-f_{cs}]}{f_l}$	Long. concrete compressive stresses (1)
$RF = \frac{0.4f'_c-0.5[f_{d1}-f_{d2}-f_{p1}-f_{p2}-f_{EL}-f_s-f_{cs}]}{f_l}$	Long. concrete compressive stresses (2)
$RF = \frac{V_{CapINV}-V_{perm}}{v_l}$	Long. principal shear web stresses
$RF = \frac{3\sqrt{f'_c}-[f_{d1}-f_{d2}-f_{p1}]}{f_l}$	Trans. top slab concrete tensile stress
$RF = \frac{0.6f'_c-[f_{d1}-f_{d2}-f_{p1}]}{f_l}$	Trans. top slab concrete compressive stress (1)
$RF = \frac{0.4f'_c-0.5[f_{d1}-f_{d2}-f_{p1}]}{f_l}$	Trans top slab concrete compressive stress (2)
Rating equation	**Strength level (LFD)**
$RF = \frac{\varnothing M_n-1.3[M_{d1}-M_{d2}-M_{p1}-M_{p2}-M_{EL}-M_s-M_{cs}}{2.17M_{L+I}}$	Long. flexural strength
$RF = \frac{\varnothing V_n-1.3[V_{uD}-V_{uT}]}{2.17V_{L+I}}$	Long. combined shear and torsional strength
$RF = \frac{\varnothing M_n-1.3[M_{d1}-M_{d2}]}{2.17M_{L+I}}$	Trans. top slab flexural strength

*f_{d1} = Stresses due to self-weight only

*f_{d2} = Stresses due to superimposed DL, parapet and Dywidag (DW)

*f_{p1} = Stresses due to primary forces from DSI PT bars

*f_{p2} = Stresses due to primary forces from External Tendons

*f_{EL} = Stresses due to secondary hyperstatic PT (DSI Bars only)

*f_{d1} = Stresses due to secondary hyperstatic PT (External Tendons only)

*f_{L+I} = Stresses due to live load plus impact

*f_{CS} = Stresses due to creep and shrinkage

*M_{d1} = Longitudinal flexural moment from self-weight

*M_{d2} = Longitudinal flexural moment from superimposed DL and WS

*M_{EL} = Longitudinal flexural moment from secondary hyperstatic PT (DSI Bars only)

*M_S = Longitudinal flexural moment from secondary hyperstatic External PT

*M_{CS} = Longitudinal flexural moment from creep and shrinkage

*M_{L+I} = Longitudinal flexural moment due to live load plus impact

*V_{CapINV} = Shear capacity at Inventory level

*V_{perm} = Unfactored summation of direct shearing forces without live load

*V_n = Nominal Shear capacity

*V_{uD} = Total shear forces obtained from self-weight, superimposed DL, secondary hyperstatic PT (DSI Bars only) and External tendon, vertical component of external tendons after losses contributing to shear resistance, and creep and shrinkage

*V_{uT} = Total longitudinal torsion obtained from self-weight, superimposed DL, secondary hyperstatic PT (DSI Bars only) and External tendon, components of external tendons after losses contributing to torsion resistance, and creep and shrinkage

*V_{l+I} = Direct shear due to live load plus impact

long as crack spacing can be identified for these members [38]. In our case, the shear capacity should be calculated along the cracked joints considering the contributions of vertical and horizontal reinforcing steel, the prestressing Dywidag bars, and the effect of the external post-tension tendons. In 1986, Vecchio and Collins [42] and based on the definitive work on the aggregate interlock mechanism of Walvren [43], derived a relationship to calculate the local shear stresses v_{ci} at a crack in the following formula:

Table 10 Operating level analysis rating cases

Rating equation	Service Level (ASD)
$RF = \frac{V_{CapOPR} - V_{perm}}{v_{1+I}}$	Long. principal web stresses
$RF = \frac{6\sqrt{f'_c} - [f_{d1} - f_{d2} - f_{p1}]}{f_l}$	Trans. top slab concrete tensile stress
Rating equation	**Strength level (LFD)**
$RF = \frac{\varnothing M_n - 1.3[M_{d1} - M_{d2} - M_{p1} - M_{p2} - M_{EL} - M_s - M_{cs}}{1.3M_{L+I}}$	Long. flexural strength
$RF = \frac{\varnothing V_n - 1.3[V_{uD} - V_{uT}]}{1.3V_{L+I}}$	Long. combined shear and torsional strength
$RF = \frac{\varnothing M_n - 1.3[M_{d1} - M_{d2}]}{1.3M_{L+I}}$	Trans. top slab flexural strength

Table 11 Inventory load rating factor summary

	Item rated	Load rating factors (RF) AASHTO HS20
Service Level (3 Lanes)	Longitudinal concrete tensile stresses bottom slab	1.74
	Longitudinal concrete tensile stresses top slab	3.34
	Longitudinal concrete compression stresses bottom slab (Compression 1)	9.05
	Longitudinal concrete compression stresses top slab (Compression 1)	17.45
	Longitudinal concrete compression stresses bottom slab (Compression 2)	6.89
	Longitudinal concrete compression stresses top slab (Compression 2)	5.18
	Transverse top slab tensile stresses	1.21
	Transverse top slab compression stresses (Compression 1)	6.35
	Transverse top slab compression stresses (Compression 2)	4.27
Strength Level (2 Lanes)	Longitudinal flexural strength	1.93
	Longitudinal web shear and torsional strength	1.27
	Transverse top slab flexural strength	1.65
	External PT steel tension	13.27

Table 12 Operating load rating factor summary

	Item rated	Load rating factors (RF) AASHTO HS20
Service Level (3 Lanes)	Longitudinal concrete tensile stresses bottom slab	2.34
	Longitudinal concrete tensile stresses top slab	4.51
	Longitudinal concrete compression stresses bottom slab (Compression 1)	12.20
	Longitudinal concrete compression stresses top slab (Compression 1)	23.54
	Longitudinal concrete compression stresses bottom slab (Compression 2)	9.29
	Longitudinal concrete compression stresses top slab (Compression 2)	13.99
	Transverse top slab tensile stresses	1.59
	Transverse top slab compression stresses (Compression 1)	6.35
	Transverse top slab compression stresses (Compression 2)	4.27
Strength Level (2 Lanes)	Longitudinal flexural strength	3.23
	Longitudinal web shear and torsional strength	2.12
	Transverse top slab flexural strength	2.76
	External PT steel tension	25.40

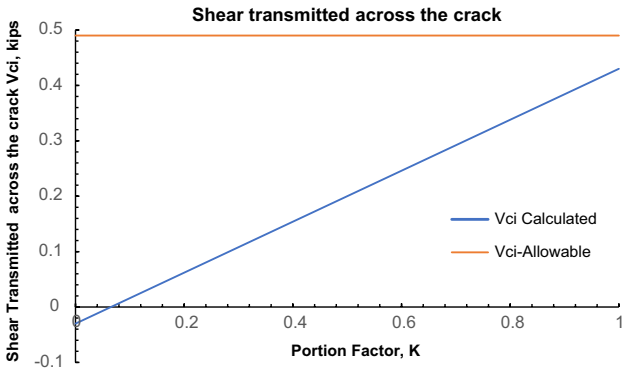

Fig. 43 Shear transmitted across the crack

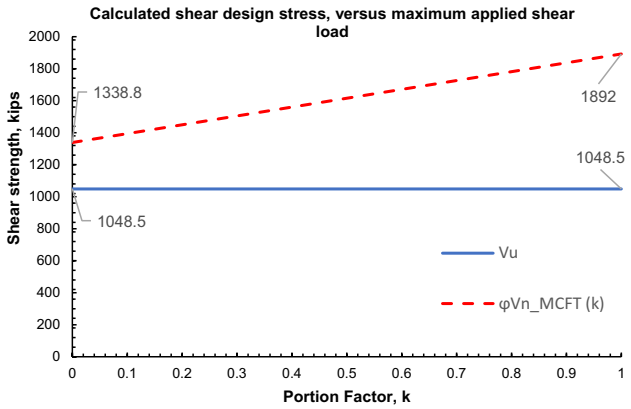

Fig. 44 Design shear strength curve, $\phi V_{n\_MCFT}(k)$ versus factored shear force

$$v_{ci} \leq \frac{0.0683\sqrt{f'_c}}{0.3 + 24w/(a_{max} + 0.63)} \tag{8}$$

Where, w = Maximum crack width (in.) measured under loading = 0.0048 *in* (0.000012192 *m*), a_{max} = Maximum aggregate size (in.) = 0.75*in*(0.019*m*), f'_c = Concrete compressive strength 7500 psi.

Then the maximum allowable shear stresses along the crack before slippage occur is:

$$v_{ci\_allowable} = \frac{0.0683 \times \sqrt{7500}}{0.3 + 24 \times \frac{0.0048}{0.75+0.63}} = 0.49 \ \text{ksi}(3.37 \text{ Mpa})$$

Collins et al. [44] derived the vertical equilibrium state, and the shear stresses occurring at the crack can be calculated using the following formula:

$$v_{ci} = \frac{A_v.f_v.\frac{d_v.\cot(\theta)}{s} + f_1.\frac{b_v.d_v}{\sin(\theta)}.\cos(\theta) - A_v.f_y.\frac{d_v.\cot(\theta)}{s}}{b_v.d_v} \tag{9}$$

where, f_v = The tensile stress in the shear reinforcement and since it is unknown, one design strategy is to assume as a fraction of f_y. Therefore, it is assumed that $f_v = k.f_y$, where k is the portion factor [41]. f_y = Steel reinforcement yield strength = 60 ksi, b_v = Effective web width = 13.34in, -A_v = Total Area of the stirrup legs resisting shear = 0.60 in^2, d_v = Effective shear depth taken as 0.72 ×h eight of the section = $0.72 \times 139.75 = 100.62in$, s = Spacing of shear reinforcement = 10 in.

$$f_1 = \textit{Average principal tensile stress in the concrete} = \frac{0.33 \times \sqrt{f'_c}}{1 + \sqrt{500 \times \varepsilon_1}} = \frac{0.33 \times \sqrt{7500}}{1 + \sqrt{500 \times 0.0002521}} = 0.25\text{ksi (1.72Mpa)} \tag{10}$$

where, ε_1 = Principal tensile strain measured at crack location = 0.0002521

Using the general procedure in AASHTO-LRFD Bridge Design Specification, 2017-Sect. 5.7.3.4.2, the new angle of inclination of the diagonal compressive stresses θ is:

$$\theta = 29 + 3500\varepsilon_s$$

where ε_s is the strain in the longitudinal reinforcement and is given by:

$$\varepsilon_s = \frac{\frac{M_u}{d_v} + 0.5N_u + \left|V_u - V_p\right| - A_{ps} \times f_{po}}{E_s \times A_s + E_p.A_{ps} + E_c.A_{ct}} \tag{11}$$

where, M_u = Total applied moment from the dead and live load on entire Sect. 80,392*kips*.ft(108,997 kN.m). N_u = Applied axial load from 138 prestressed Dywidag bars of 1.25 in^2 each. V_u = calculated factored shear force for the bridge = 2,175*kips* (9,675 kN). V_p = Shear force component due to external prestress force in the vertical direction, = 361.16*kips* (1606 kN). A_{ps} = Total area of prestressing steel on the flexural tension side consisting of 12 post-tension strands of 0.217in^2 each and an additional 100 pre-tensioned Dywidag bars of 1.25in^2 each. E_c = Concrete modulus of elasticity = $33{,}000.145^{\frac{3}{2}}.\sqrt{f'_c}$ = 4989.95 ksi A_{ct} = area of concrete in tension = 55ft^2, f_{po} = Is a parameter taken as the modulus of elasticity of prestressing steel multiplied by the locked-in difference in strain between the prestressing steel and the concrete surrounding (ksi) = 0.7 f_{pu} = 189*ksi* 1,303 Mpa. E_s = Steel elastic modulus = 29, 000 ksi(200,000 Mpa). A_s = 0in^2(only prestressing steel is used in the longitudinal reinforcement). E_p = Prestressed strand modulus of elasticity = 28,500 ksi (196,500 Mpa).

The strain in the longitudinal reinforcement is:

$$\varepsilon_s = \frac{\frac{M_u}{d_v} + 0.5N_u + \left|V_u - V_p\right| - A_{ps} \times f_{po}}{E_s \times A_s + E_p.A_{ps} + E_c.A_{ct}}$$

$$\varepsilon_s = -0.00012$$

The AASHTO LRFD Sect. 5.7.3.4.2, state that the strain in the longitudinal reinforcement should meet the following conditions:

$$M_u \geq \left|V_u - V_p\right| d_v \tag{12}$$

$$80{,}392 \geq |2{,}175 - 361.6| x 8.385$$

$$80{,}392\text{kips.ft} \geq 15{,}202 kips.\text{ft}.$$

And if the value of $\varepsilon_s < 0$, it should be taken as 0.

Then the new angle of inclination θ is:

$$\theta = 29 + 3500\varepsilon_s = 29° \tag{13}$$

The factor indicating the ability of diagonally cracked concrete to transmit tension and shear, β is:

$$\beta = \frac{4.8}{\left(1 + 750\varepsilon_s\right)} = 4.8 \tag{14}$$

The variation of the shear transmitted across the crack in terms of f_y is plotted in Fig. 43, along with the maximum allowable shear stress $v_{ci\_allowable}$. When the tensile stress in the shear reinforcement, f_v reach f_y, the shear transmitted across the crack is equal to 0.43 ksi, less than the maximum allowable shear. As a result, no crack slippage occurs along the crack.

9 MCFT application to determine the concrete shear capacity across the crack

The shear resistance from the concrete and the web reinforcement on a single web using the MCFT equation from Design of Highway Bridges an LRFD, Eq. 7.132 for shear is:

$$V = f_1 b_v d_v \cot(\theta) + \frac{2.A_v f_v d_v}{s} \cot(\theta) \tag{15}$$

$$= 1{,}922\, kips\ (8549\text{kN})$$

where V represents the sum of the contributions of the shear resistance on a single web, concrete, and web reinforcement equilibrium condition.

The design shear capacity of the bridge derived analytically from AASHTO LRFD Eq. 5.7.3.3-1 is:

$$\phi V_n = \phi(V_c + V_s + 0.5.V_p) \tag{16}$$

where V_c = Nominal shear strength in concrete on a single web

$$= 0.0316\ \beta.\lambda.\sqrt{f'_c}.b_v.d_v, \lambda = 1) \tag{17}$$

$$= 557.57\ \text{ kips } (2480.20\ \text{ kN}).$$

V_s = Nominal shear strength of the reinforcement on a single web

$$= \frac{A_v \times f_y \times d_v(\cot\theta + \cot\alpha)\sin\alpha}{s} \tag{18}$$

where α is the transverse reinforcement inclination angle $= 90°$

$$V_s = 1307\, kips\ (5{,}813.8\ \text{kN})$$

V_p = Component of prestressing force in the direction of the shear force V_p:

$$V_p = 12.F_p.(\sin(\alpha 1) + \sin(\alpha 2)) \tag{19}$$

where

$$\alpha 1 = Tendonangle\ near\ the\ pier = 9°$$
$$\alpha 2 = Tendonangle\ near\ the\ pier = 16°$$
$$F_p = Shear\ force\ calculated\ in\ post\ tensioned\ strands = 12.A_{ps}.\left(0.75.f_{pu} - Losses\right)$$
$$f_{pu} = Ultimate\ stress\ of\ prestressing\ strand = 270ksi$$
$$A_{ps} = Area\ of\ presstressing\ steel\ in\ the\ section = 0.217in^2 \tag{20}$$

Then the total prestressing force V_p is:

$$V_p = 361.16kips(1{,}606kN)$$

Therefore, the total design shear strength calculated from the AASHTO LRFD is:

$$\phi V_n = \phi\left(V_c + V_s + V_p/2\right) = 1840\,kips\ (8187kN).$$

On the other hand, the total shear capacity calculated from the MCFT method resulted in:

$$\begin{aligned} V_{n\_MCFT} &= f_1 b_v d_v \cot(\theta) + \phi\frac{2.A_v f_v d_v}{s}\cot(\theta) + \frac{\phi V_p}{2} \\ &= 615 + 1{,}176 + 180.6 \\ &\quad (8767.45kN) \end{aligned} \tag{21}$$

Comparing the results from the two methods indicates that although the web section is cracked, the shear capacity in concrete remains strong. The concrete shear capacity ($f_1 b_v d_v \cot(\theta)$) derived from the PLT is 23% higher than the design shear strength of the concrete (ϕV_c) calculated using AASHTO LRFD method.

The total shear force on a single web $V_{u,1w}$ is equal to:

$$V_{u,1w} = \left(V_{LL,1w} + V_{DL,1w}\right) \tag{22}$$

Where $V_{LL,1w}$ = calculated shear force due to live load from highest truck loading (300 kips) at Pier #4 = $40kips$. $V_{DL,1w}$ = calculated shear force due to dead load on single web = $1009kips$.

Then

$$V_{u,1w} = 1088\,kips$$

Assuming that the design of concrete shear strength is a portion of k, the total design shear strength of a single web can be summarized in the following equation:

$$\phi V_{n\_MCFT}(k) = \phi\left(k.f_1 b_v d_v \cot(\theta) + V_s + 0.5V_p\right) \tag{23}$$

Figure 44 below shows that the design shear strength curve $\phi V_{n\_MCFT}(k)$, varies from 1338.8 kips to 1892 kips, demonstrating that even if the concrete shear design capacity in the web is neglected, the bridge design shear strength ϕV_{n_MCFT} is still approximately 30% higher than the total shear force. Also, the calculation shows that the design shear capacity of the bridge ϕV_{n_MCFT} is 1.8 times stronger than the total applied shear force $V_{u,1w}$.

10 Summary and conclusion

A proof loading test was successfully completed for four different loadings and unloading phases to assess structural behavior for I-39 Kishwaukee River Bridge. The maximum testing load of 136 tons was produced by two trucks crossing the bridge side by side (68 Tons from each truck). The proof load test consisted of 9 critical positions with 11 different tests. 48 strain gauges, 16 crackmeters, and 5 LVDTs were distributed along the first three spans of the bridge. The bridge showed no signs of distress, with high stability and consistent linear elastic behavior. In addition, the modified compression field theory was used to assess the bridge concrete shear capacity at the cracked section of the web. To ensure the success of the PLT, the paper recommend the followings:

1. A finite element analysis software is recommended to find the target proof load sufficient to encompass any future live load factor, L_T, from vehicles (mainly trucks) and dynamic load allowance without causing permanent damage to the bridge.
2. Prior to testing, a finite element or structural analysis is the key to determine the critical locations where the highest response is detected for flexural, shear, and displacement. Sensors should be placed only at points of maximum response
3. Another key factor to consider before instrumenting the bridge is the sensor type, model, size, and accuracy to ensure good results with an acceptable error range. The sensor selection study should take into consideration the material property, material composition (Homogeneity or heterogeneity), surrounding temperature, humidity, and load application.
4. During proof loading, a Real-Time monitoring should be considered especially when any significant slope decrease is observed during load increase.
5. The Bridge rating of segmental structures depend on rating of each segment.

The findings, and conclusions that can be drawn from this study are:

1. The bridge safety assessment using proof load testing is considered a more reliable method than Diagnostic Load Testing when calculating the reserve capacity of the bridge because it shows the real bridge behavior under a magnified live load that takes into account the dynamic and overload effect. Also, PLT doesn't rely on assumptions one needs to make to calibrate the model due to possible lack of documentation, concrete delamination, or inaccurate reinforcement plans.
2. For proof load testing, the sensors should be placed only at points of maximum response.
3. Moment-strain curves, deflection readings, and crack growth tracking were used as a measure to observe the linear elastic behavior and capture any odd behavior during load testing. A linear elastic behavior validation also

requires all the sensors to return to their original reading values once the loading is removed, which conforms with testing results.

4. When concrete structure exhibits cracks and discontinuities, instead of simply neglecting the contribution of concrete to the shear capacity of the bridge, the Modified Compression Field theory provides a clear direction on the internal mechanism of cracked concrete's contribution to shear resistance. The MCFT demonstrated that the bridge concrete shear capacity at the cracked locations remains strong and active.
5. Proof Load Testing for the Kishwaukee bridge was concluded using LFD and ASD methods for bridge load rating. All bridge segments received a Rating Factor higher than 1 for both Inventory and Operating levels for all different testing scenarios, proving the bridge is safe.
6. This study showed that the shear capacity of the bridge is 1.8 times stronger than the total applied shear force obtained from the bridge dead load and 136 Tons of truck live load. This concludes that the Kishwaukee I-39 bridge remains safe for future traffic load increases or higher truck loads.

Appendix

1. Instrumented sections plans

See appendix Fig. 45, 46, 47, 48, 49, 50, 51, 52, 53, 54.

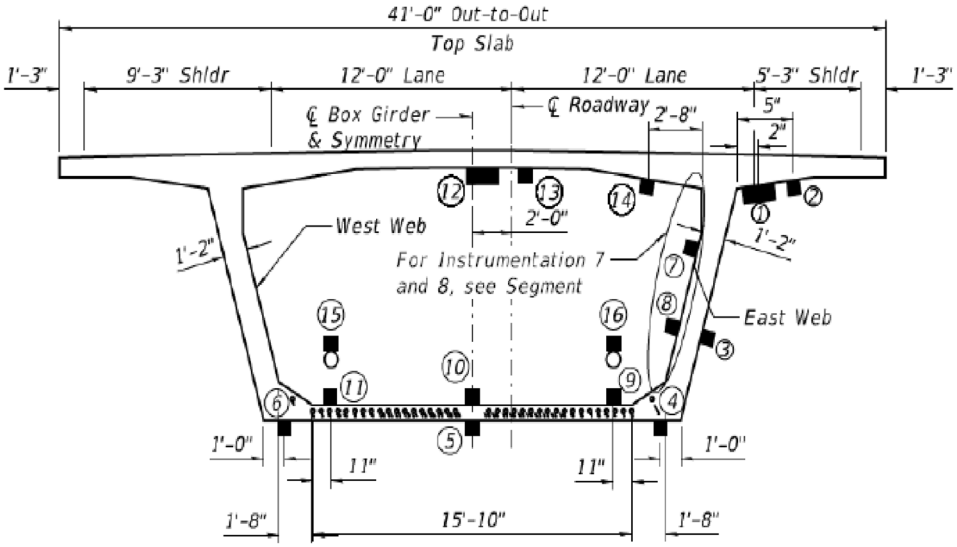

Fig. 45 Strain gauges installed at Span #5 for maximum positive moment

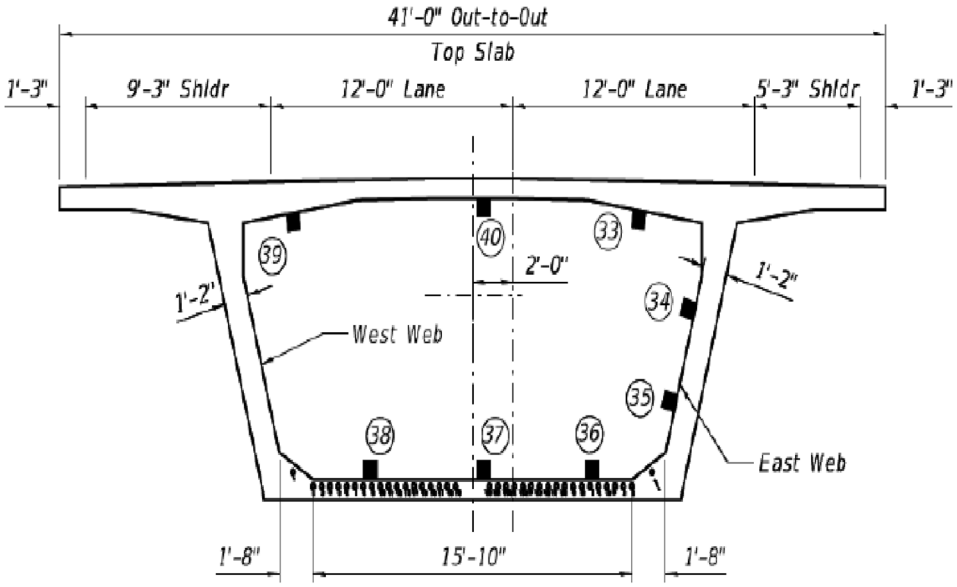

Fig. 46 Strain gauges installed at mid-Span #4 for maximum positive moment

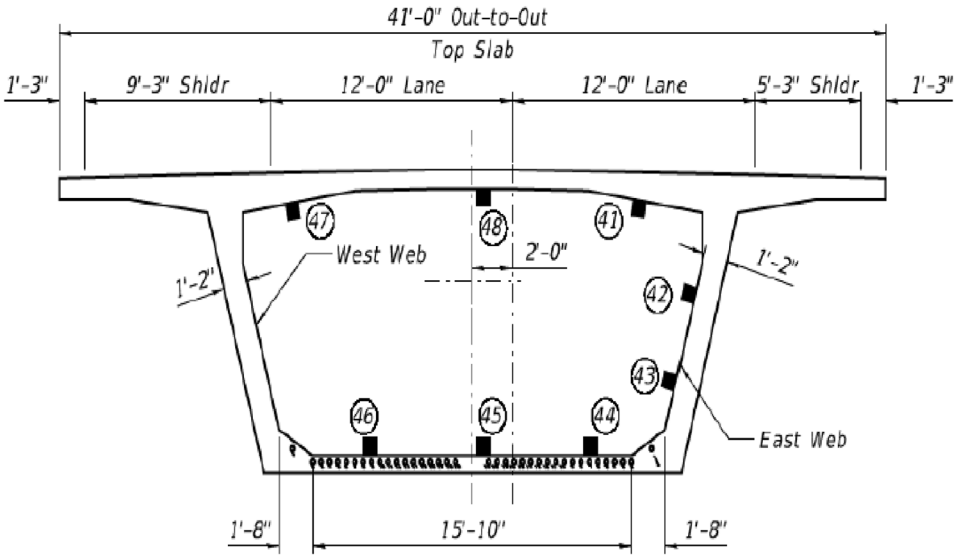

Fig. 47 Strain gauges installed at mid-Span #3 for maximum positive moment

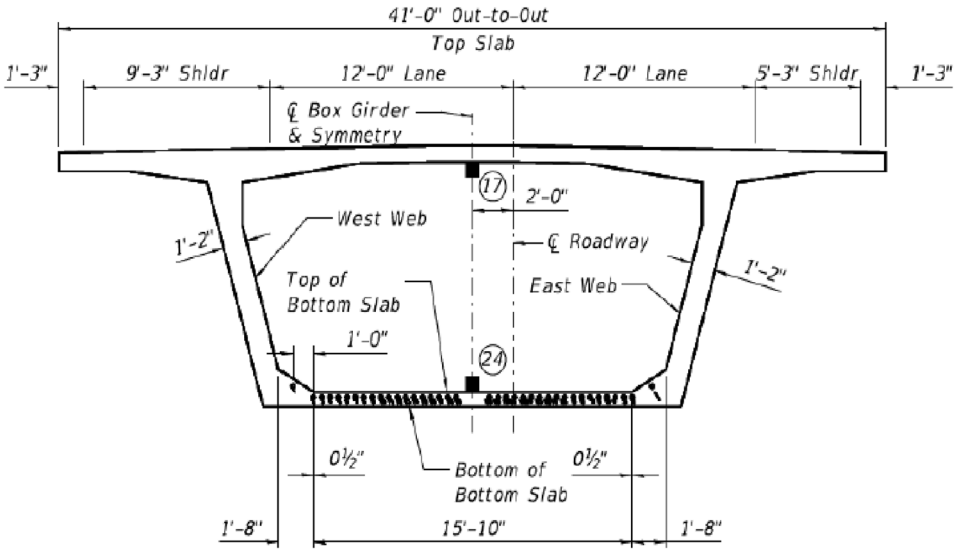

Fig. 48 Strain gauges installed at Pier #4 for the maximum negative moment (SB-S1 section)

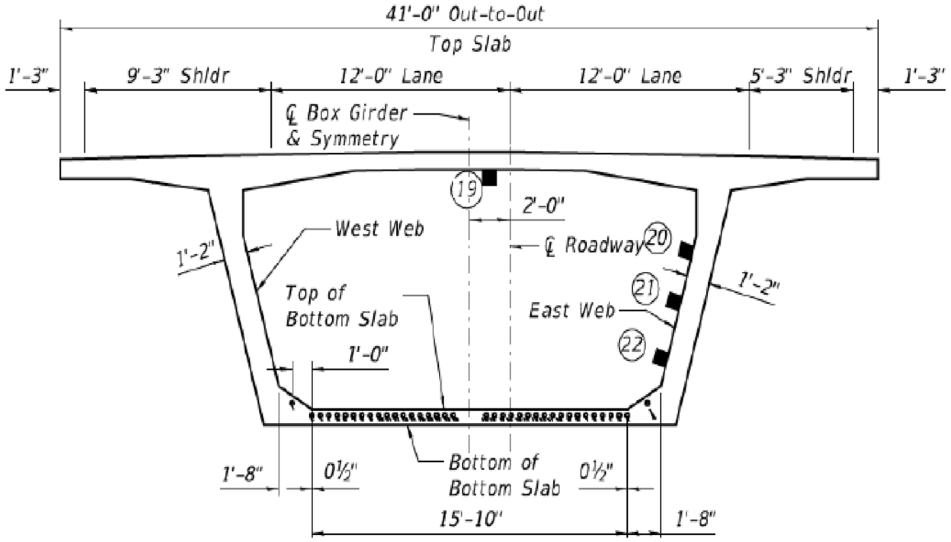

Fig. 49 Strain gauges installed at Pier #4 for the maximum negative moment (SB4-S2 section)

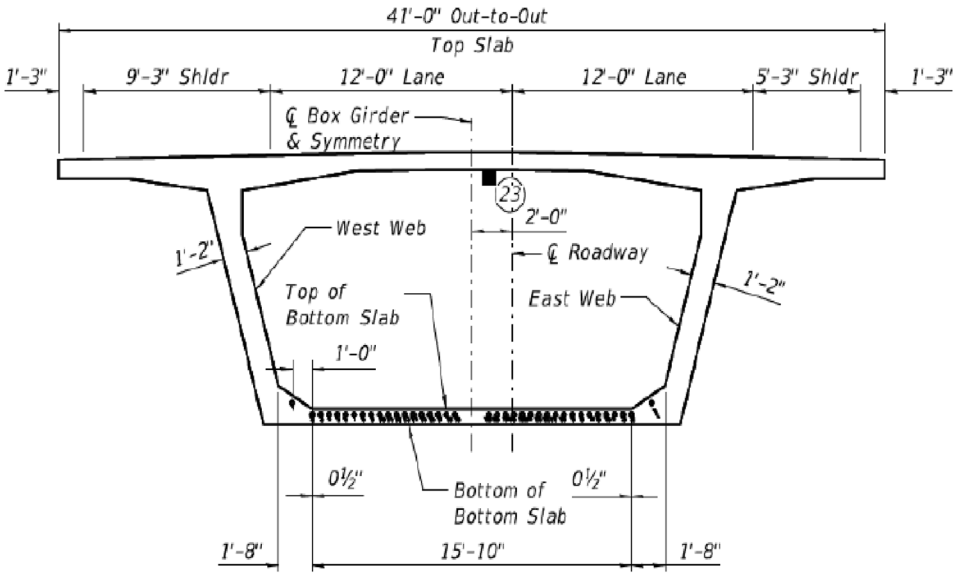

Fig. 50 Strain gauges installed at Pier #4 for the maximum negative moment (SB4-N0 & SB4-S0 section)

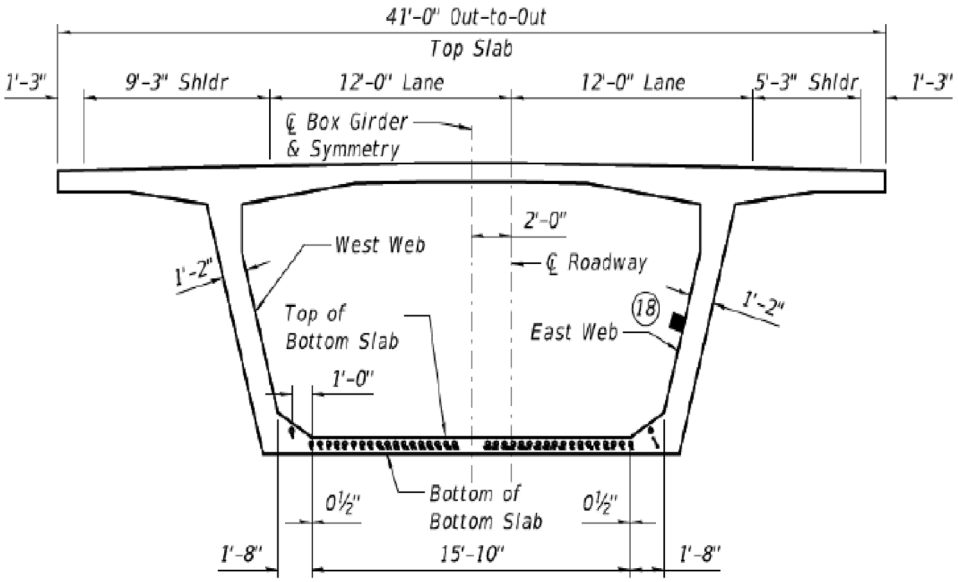

Fig. 51 Strain gauges installed at Pier #4 for the maximum negative moment (SB4-N2 section)

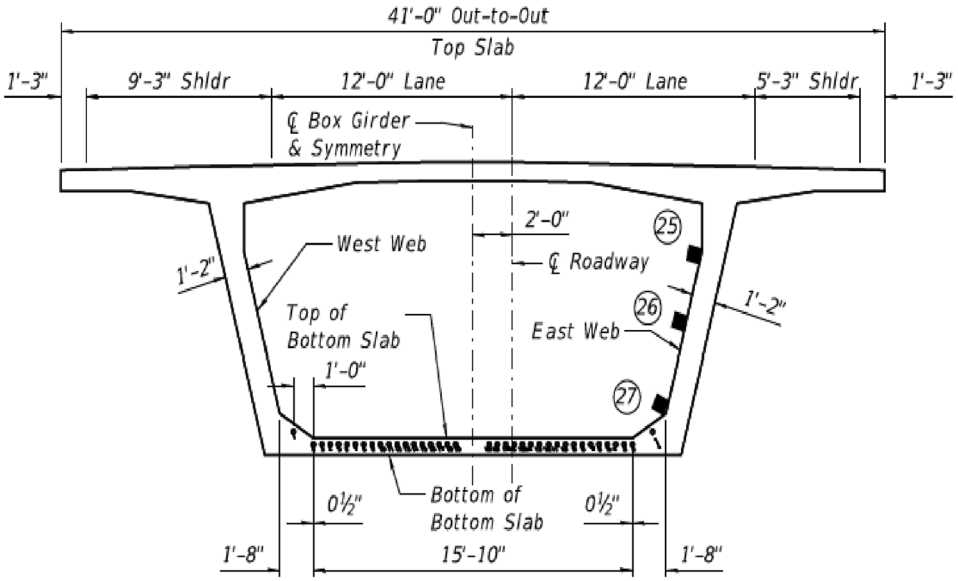

Fig. 52 Strain gauges installed at Pier #3 for the maximum negative moment (SB3-N1 section)

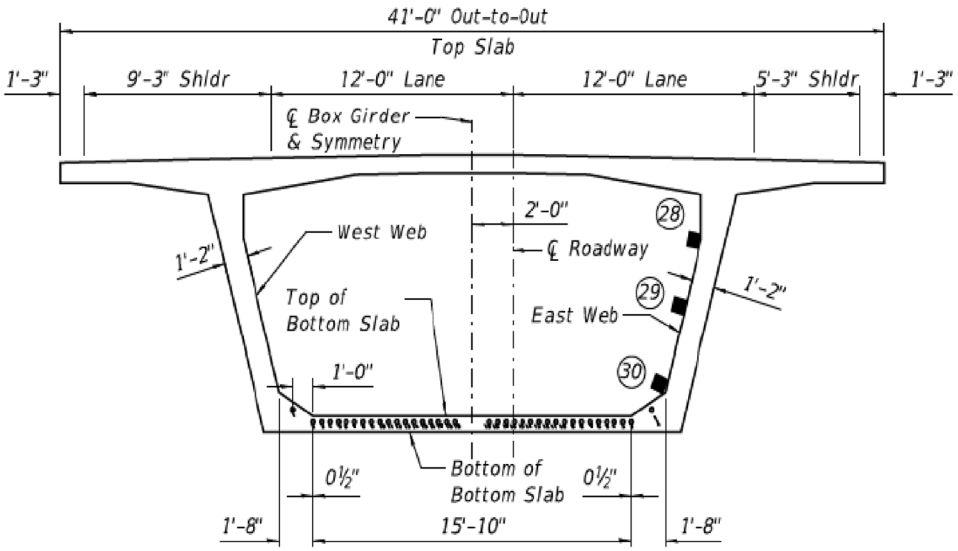

Fig. 53 Strain gauges installed at Pier #3 for the maximum negative moment (SB3-S1 section)

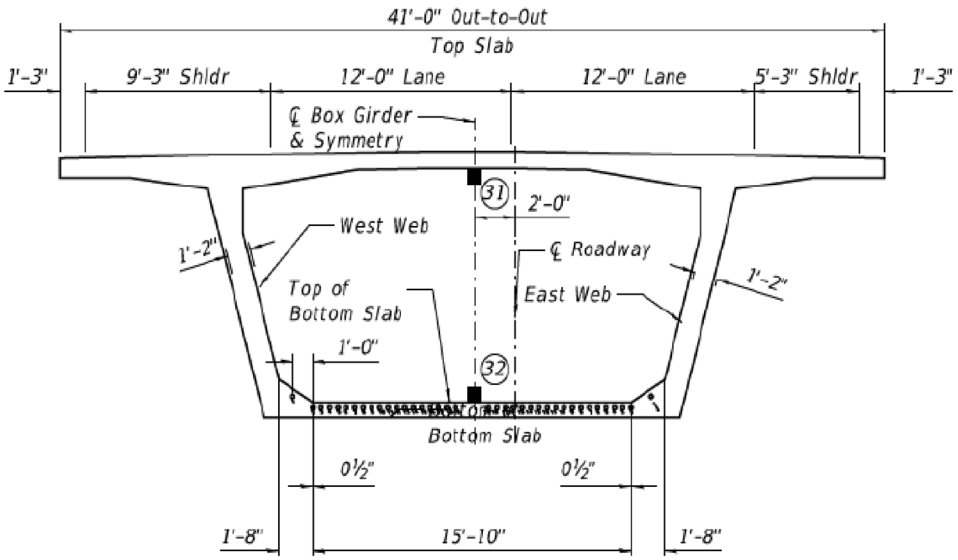

Fig. 54 Strain gauges installed at Pier #3 for the maximum negative moment (SB3-N0 & SB3-S0 sections)

2. Strain gauges readings

See appendix Fig. 55, 56, 57, 58, 59, 60, 61, 62, 63, 64.

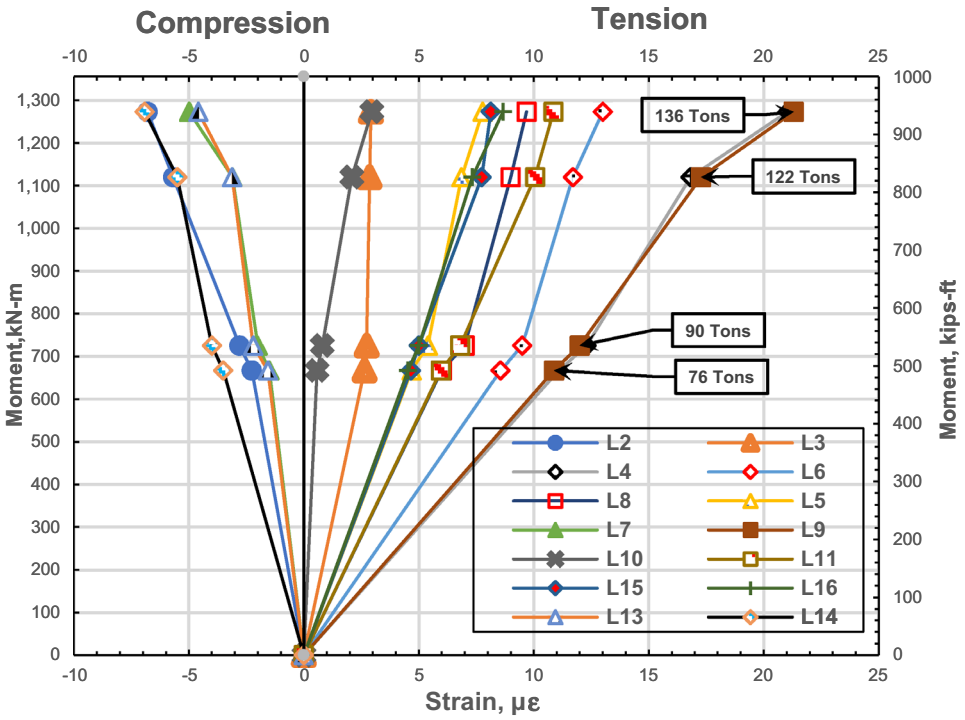

Fig. 55 Moment versus peak strain in compression and tension at 0.4 L of span 5

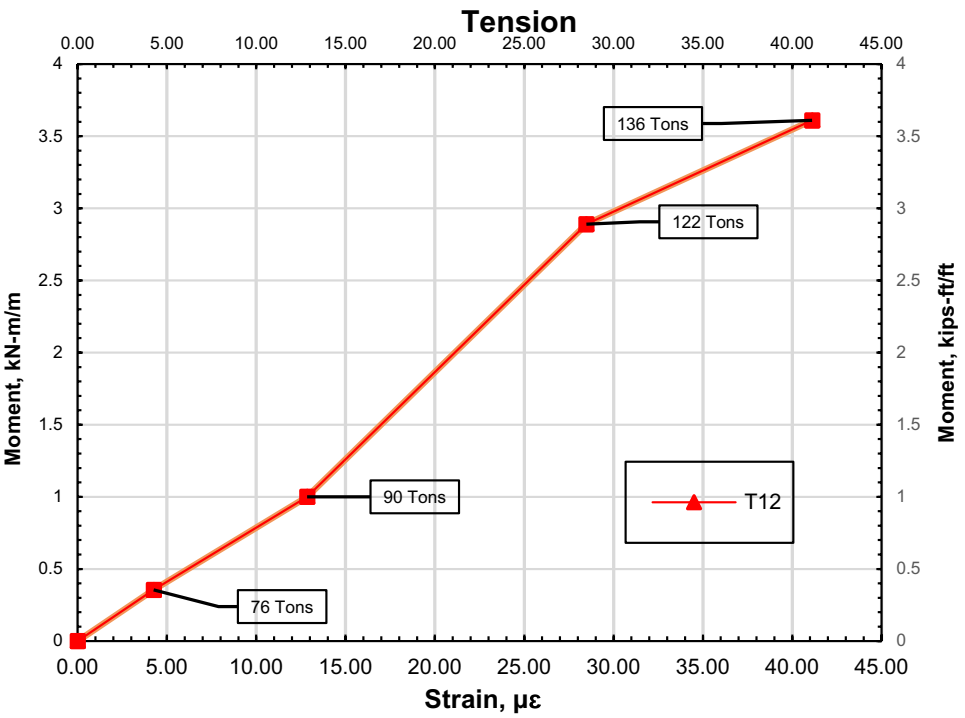

Fig. 56 Moment versus peak strain in compression and tension at 0.4 L of span 5

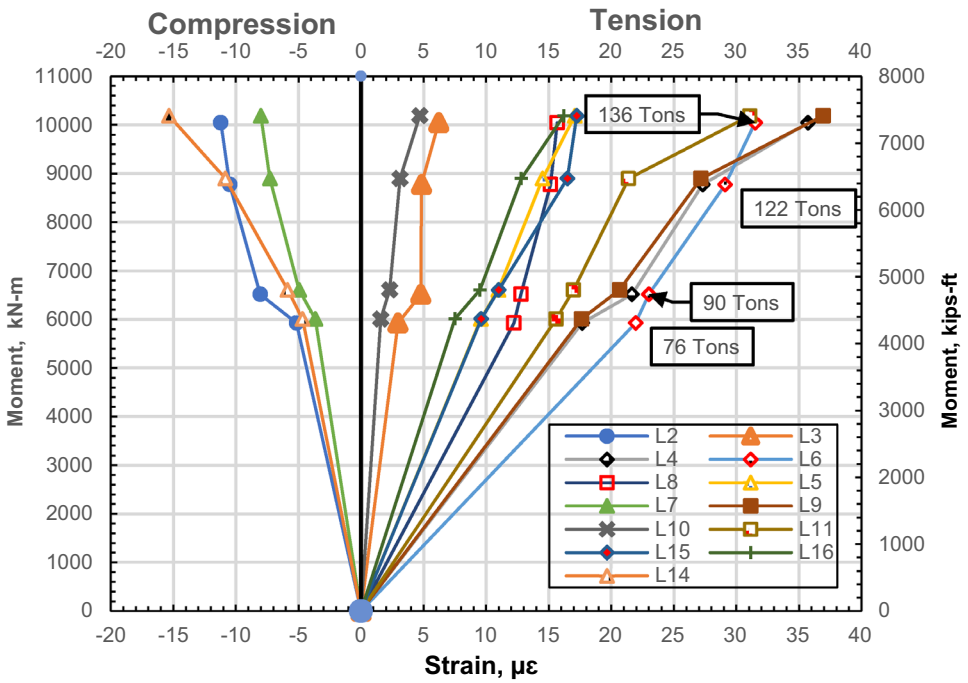

Fig. 57 Moment versus peak strain curves in compression and tension at Pier #4 SB4-S2 section

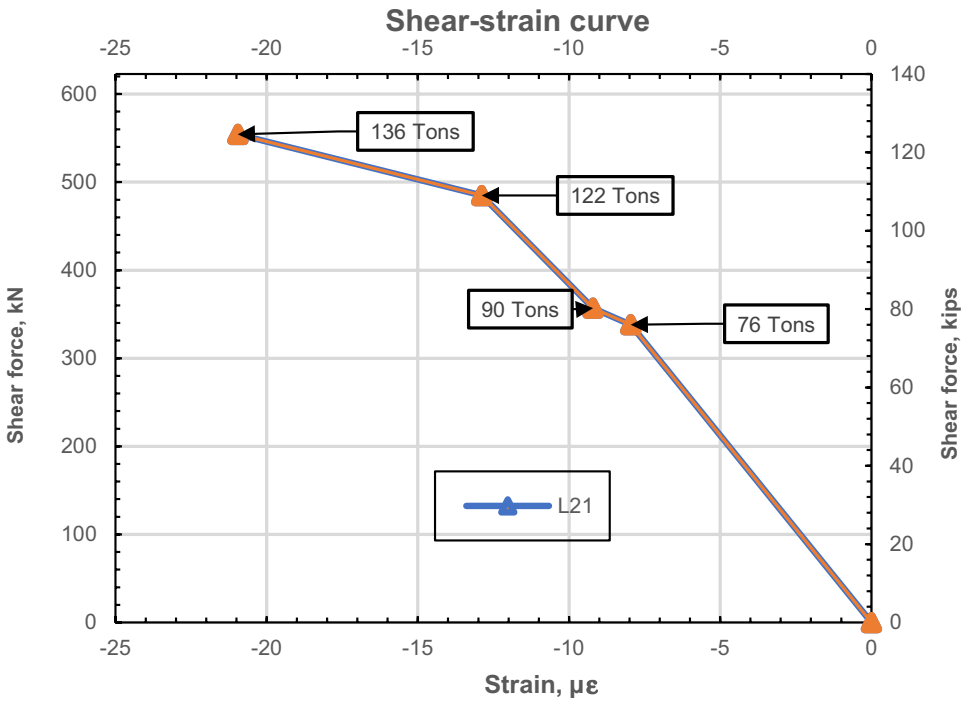

Fig. 58 Moment versus peak strain curves in compression and tension at Pier #4 SB4-S1 section

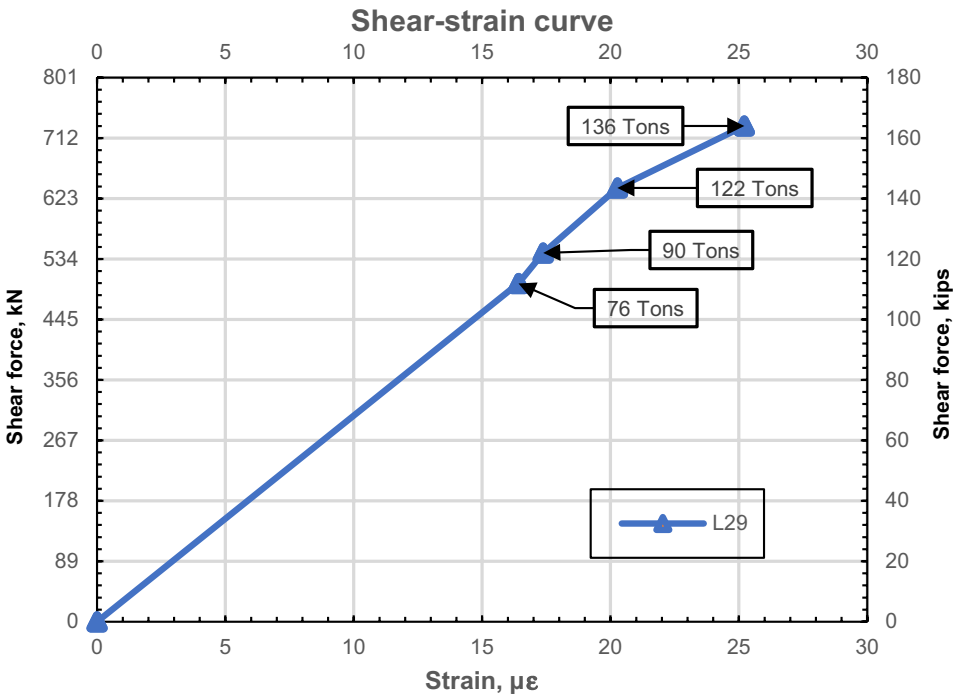

Fig. 59 Moment versus peak strain curves in compression and tension at Pier #3, SB3-N1 section

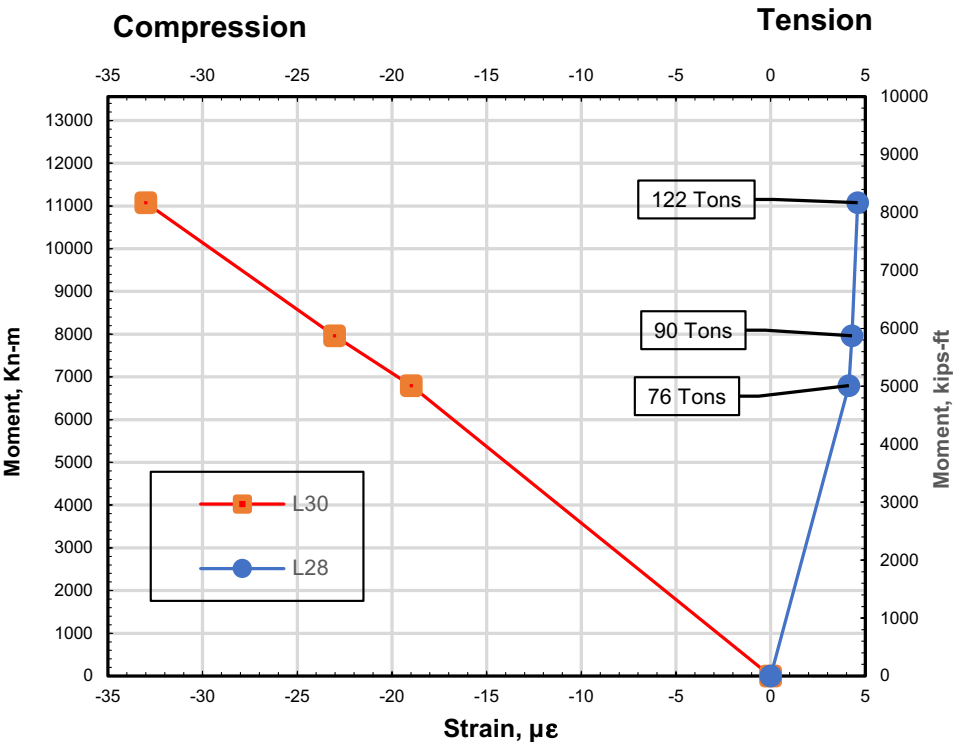

Fig. 60 Moment versus peak strain curves in compression and tension at Pier #3, SB3-S1 section

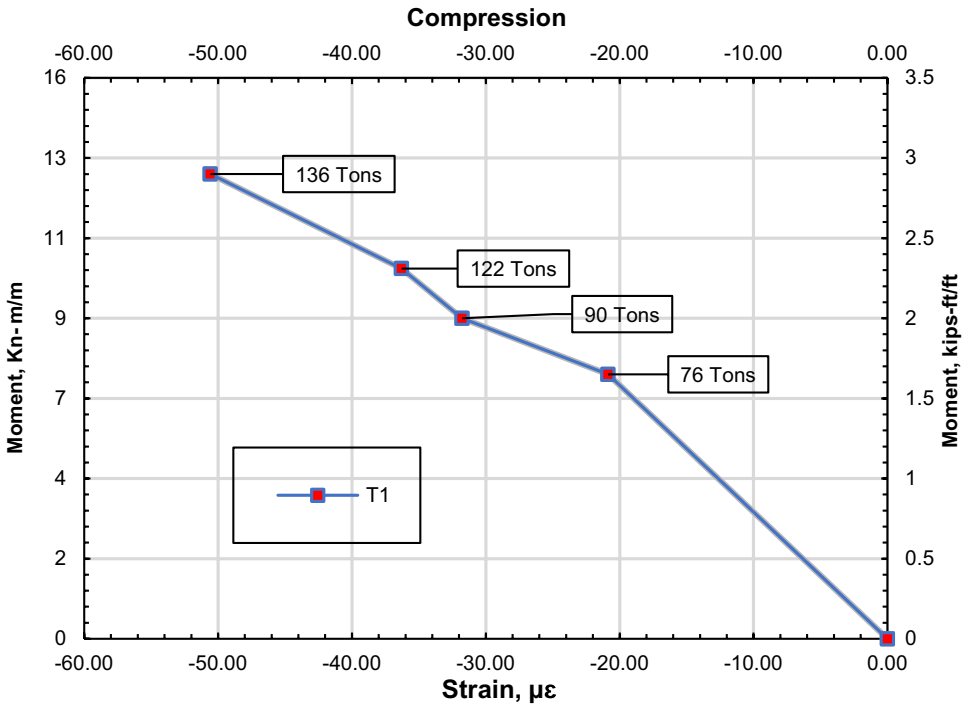

Fig. 61 Torsion moment versus peak strain curves in compression curves for T1 strain gauges located at 0.4L of Span #5

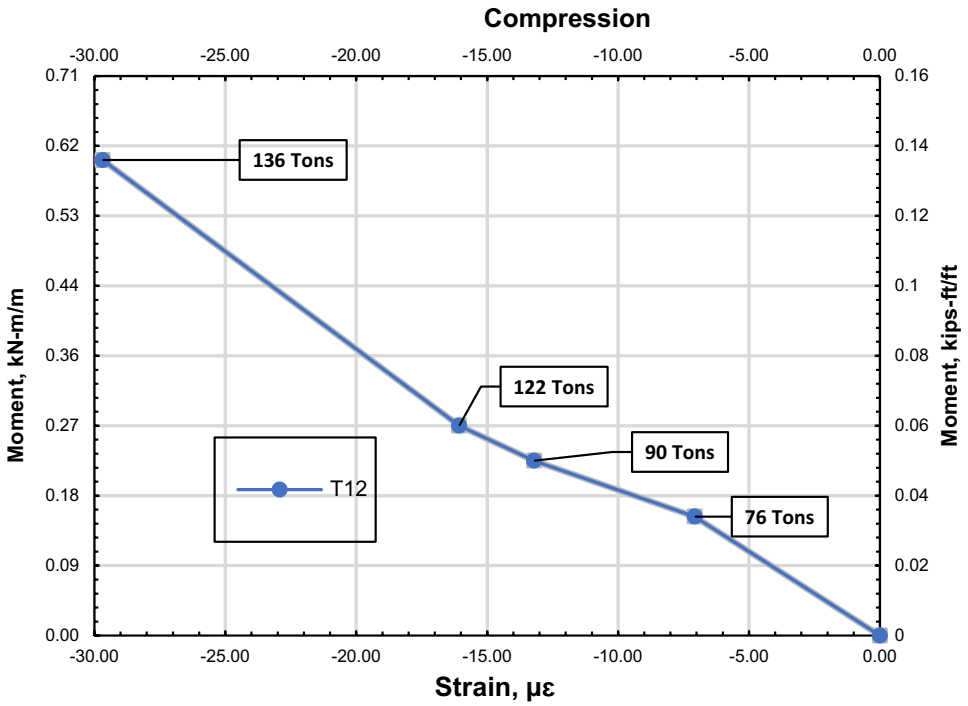

Fig. 62 Torsion moment versus peak strain curves in compression curves for T12 strain gauges located at 0.4L of Span #5

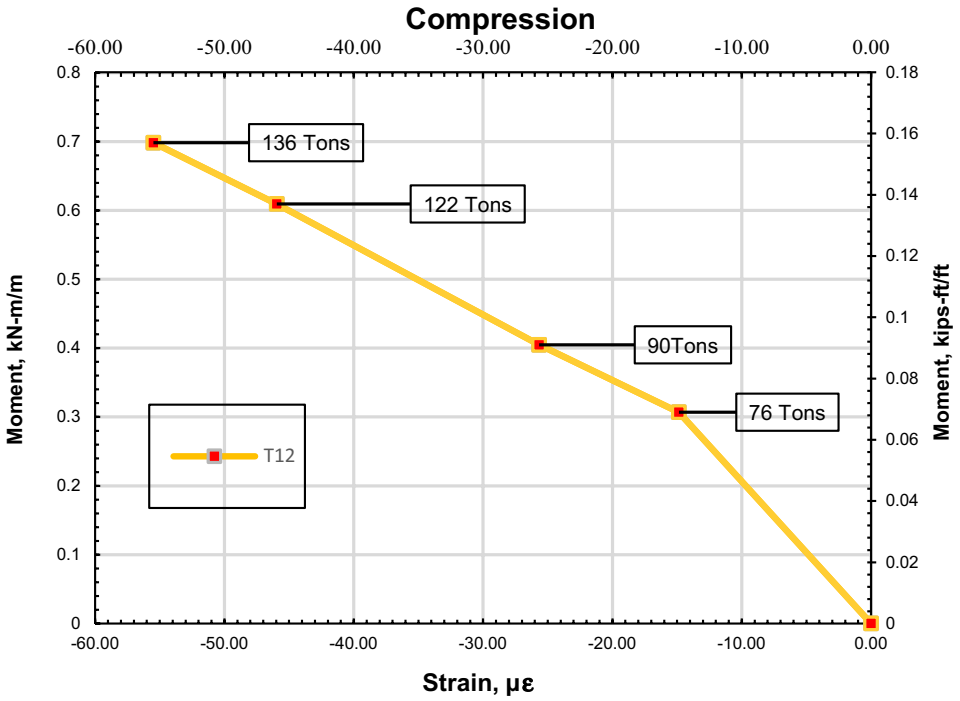

Fig. 63 Moment-strain curves for transversal strain gauge T12 located at 0.4L of Span #5

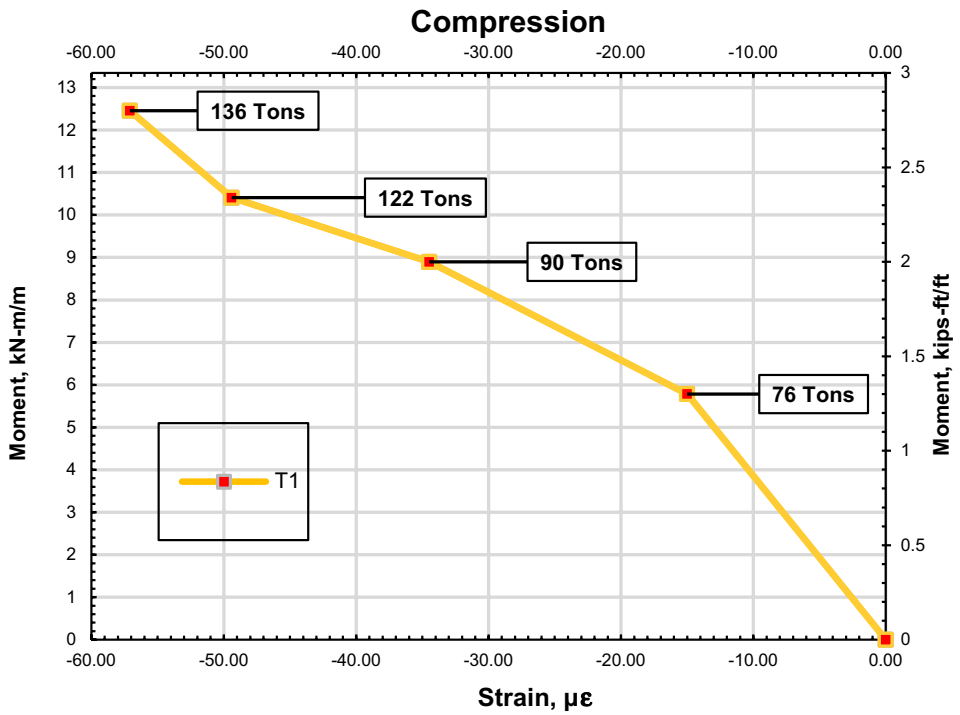

Fig. 64 Moment-strain curves for transversal strain gauge T1 located at 0.4L of Span #5

Acknowledgements The authors would like to thank Illinois Department of Transportation (IDOT) and HBM Engineering Group for funding this project. Thanks are due to Mr. Mahmoud Etimadi, bridge maintenance engineer, District 2, IDOT and Dr. Moussa Issa, Chief structural engineer, HBM Engineering Group, LLC and his team for their efforts in project management and field-testing coordination. I would like to thank the university of Illinois (UIC) research team, Mohammad Mahdi and Masoud Rezaei led by Professor Mohsen Issa.

Data availability The datasets generated during and/or analysed during the current study are available from the corresponding author on reasonable request.

References

1. Ransom, A., and R. J. Heywood. "Recommendations for Proof Load Testing in Australia." In *AUSTROADS BRIDGE CONFERENCE, 1997*, vol. 1. 1997.
2. United States. Federal Highway Administration. 2011. Our Nation's Highways 2011. 2011. FHWA-PL-11–028. https://rosap.ntl.bts.gov/view/dot/50502.
3. Sanayei, M., Reiff, A. J., Brenner, B. R., & Imbaro, G. R. (2016). Load Rating of a Fully Instrumented Bridge: Comparison of LRFR Approaches. *Journal of Performance of Constructed Facilities*, *30*(2). https://doi.org/10.1061/(asce)cf.1943-5509.0000752
4. Naser, A. F., Mohammed, H. A., & Mohammed, A. A. (2022). Flexure and shear load rating evaluation of composite bridge superstructure under effect of different trucks load types. *Materials Today: Proceedings*, 398–407. https://doi.org/10.1016/j.matpr.2021.12.268
5. S. Gordon and D. O'Connor, "BRIDGE MANAGEMENT, EVALUATION, AND REHABILITATION: A SURVEY OF CURRENT PRACTICE," in BRIDGE REHABILITATION. PROCEEDINGS OF THE 3RD INTERNATIONAL WORKSHOP ON BRIDGE REHABILITATION, JUNE 14–17, 1992, ORGANIZED BY THE TECHNICAL UNIVERSITY DARMSTADT AND THE UNIVERSITY OF MICHIGAN, Berlin, 1992.
6. Narayanan, S. (2008). *I-35W Mississippi river bridge failure-Is it a wake up call? Cold-formed Steel Built-up Beams View project Creative Writing View project*. https://www.researchgate.net/publication/292870482
7. FDOT. 2015. "Florida Department of Transportation Bridge Load Rating." http://www.dot.state.fl.us/statemaintenanceoffice/LoadRating.shtm.
8. Alampalli, S., Frangopol, D. M., Grimson, J., Halling, M. W., Kosnik, D. E., Lantsoght, E. O. L., Yang, D., & Zhou, Y. E. (2021). Bridge Load Testing: State-of-the-Practice. Journal of Bridge Engineering, 26(3). https://doi.org/10.1061/(asce)be.1943-5592.0001678
9. Barker MG (2001) Quantifying field-test behavior for rating steel girder bridges. J Bridg Eng 6(4):254–261
10. Lantsoght EOL, Koekkoek RT, Hordijk D, de Boer A (2018) Towards standardisation of proof load testing: pilot test on viaduct Zijlweg. Struct Infrastruct Eng 14(3):365–380. https://doi.org/10.1080/15732479.2017.1354032
11. Nilimaa J, Bagge N, Blanksvärd T, Täljsten B (2015). NSM CFRP Strengthening and Failure Loading of a Posttensioned Concrete Bridge. https://doi.org/10.1061/(ASCE)CC.1943
12. Puurula, A. M., Enochsson, O., Sas, G., Blanksvärd, T., Ohlsson, U., Bernspång, L., Täljsten, B., Carolin, A., Paulsson, B., & Elfgren, L. (2015). Assessment of the Strengthening of an RC Railway Bridge with CFRP Utilizing a Full-Scale Failure Test and Finite-Element Analysis. *Journal of Structural Engineering*, *141*(1). https://doi.org/10.1061/(asce)st.1943-541x.0001116
13. Shifferaw Y, Fanous FS (2013) Field testing and finite element analysis of steel bridge retrofits for distortion-induced fatigue. Eng Struct 49:385–395. https://doi.org/10.1016/j.engstruct.2012.11.023
14. Aguilar, C. v., Jáuregui, D. v., Newtson, C. M., Weldon, B. D., & Cortez, T. M. (2015). Load rating a prestressed concrete double t-beam bridge without plans by field testing. In *Transportation Research Record* (Vol. 2522, pp. 90–99). National Research Council. https://doi.org/10.3141/2522-09
15. Anay, R., Cortez, T. M., David, ;, Jáuregui, V., Asce, M., Elbatanouny, M. K., & Ziehl, P. (2015a). *On-Site Acoustic-Emission Monitoring for Assessment of a Prestressed Concrete Double-Tee-Beam Bridge without Plans*. https://doi.org/10.1061/(ASCE)CF.1943
16. Shenton, H. W., Michael J. Chajes, and J. Huang. "Load rating of bridges without plans." *V. DCT* 195 (2007).
17. Jáuregui D, v., & Barr, P. J. (2004) Nondestructive Evaluation of the I-40 Bridge over the Rio Grande River. J Perform Constr Facil 18(4):195–204. https://doi.org/10.1061/(asce)0887-3828(2004)18:4(195)
18. Wang, Ming L. "Long term health monitoring of post-tensioning box girder bridges." (2004).
19. Nair, R. Shankar, and James K. Iverson. "Design and construction of the Kishwaukee river bridge." *PCI JOURNAL* 27, no. 6 (1982): 22–47.
20. Furrer, Martin, and Mahmoud Etemadi. "Strengthening of the I-39 Bridges over the Kishwaukee River." In *17th IABSE Congress: Creating and Renewing Urban Structures–Tall Buildings, Bridges and Infrastructure, Chicago, USA, 17–19 September 2008*, pp. 202–203. 2008.
21. Moussa, Y., Issa, A., Shahawy, M. A., Issa, M. A., Mohsen, P. E., Shahawy, A., & Structural Analyst, P. E. (1993). *DYNAMIC AND STATIC TESTS OF PRESTRESSED CONCRETE GIRDER BRIDGES IN FLORIDA*.
22. WSDOT. 2022. "Chapter 13 Bridge Load Rating - Bridge Design Manual M 23–50.
23. Alampalli, Sreenivas, Dan M. Frangopol, Jesse Grimson, David Kosnik, Marvin Halling, Eva OL Lantsoght, Jeff S. Weidner, David Y. Yang, and Y. Edward Zhou. "Primer on bridge load testing." *Transportation Research Circular* E-C257 (2019).
24. AASHTO (2018) The Manual for Bridge Evaluation, 3rd edn. American Association of State Highway and Transportation Officials, Washington, DC
25. Commander, B. (2019). Evolution of bridge diagnostic load testing in the USA. In *Frontiers in Built Environment* (Vol. 5). Frontiers Media S.A. https://doi.org/10.3389/fbuil.2019.00057
26. Zarate Garnica GI, Lantsoght EOL, Yang Y (2022) Monitoring structural responses during load testing of reinforced concrete bridges: a review. Struct Infrastruct Eng 18(10–11):1558–1580. https://doi.org/10.1080/15732479.2022.2063906
27. Faber MH, Val DV, Stewart MG (2000) Proof load testing for bridge assessment and upgrading. Eng Struct 22(12):1677–1689
28. Casas JR, Gómez JD (2013) Load rating of highway bridges by proof-loading. KSCE J Civ Eng 17(3):556–567. https://doi.org/10.1007/s12205-013-0007-8
29. Bakht B, Jaeger LG (1990) Bridge testing—A surprise every time. J Struct Eng 116(5):1370–1383
30. Favre, R., M. Hassan, and I. Markey. "Bridge behaviour drawn from load tests." In *BRIDGE REHABILITATION. PROCEEDINGS OF THE 3RD INTERNATIONAL WORKSHOP ON BRIDGE REHABILITATION, JUNE 14–17, 1992, ORGANIZED BY THE TECHNICAL UNIVERSITY DARMSTADT AND THE UNIVERSITY OF MICHIGAN*. 1992.
31. Moses, Fred, Jean Paul Lebet, and Rolf Bez. "Applications of field testing to bridge evaluation." *Journal of Structural Engineering* 120, no. 6 (1994): 1745–1762.
32. Comisu CC, Taranu N, Boaca G, Scutaru MC (2017) Structural health monitoring system of bridges. Procedia Engineering 199:2054–2059. https://doi.org/10.1016/j.proeng.2017.09.472
33. Coletti DA (2002) Analytical and field investigation of Roma suspension bridge. J Bridg Eng 7(3):156–165
34. Chen Y, Corr DJ, Durango-Cohen PL (2014) Analysis of common-cause and special-cause variation in the deterioration of transportation infrastructure: A field application of statistical process control for structural health monitoring. Transportation Research Part B: Methodological 59:96–116. https://doi.org/10.1016/j.trb.2013.11.002
35. Zhou, Y. E., & Guzda, M. R. (2020). Bridge Load Rating Through Proof Load Testing for Shear at Dapped Ends of Prestressed

Concrete Girders. *Frontiers in Built Environment*, *6*. https://doi.org/10.3389/fbuil.2020.00117
36. Lloyd, G. M., Wang, M. L., & Wang, X. (2004). Thermomechanical analysis of the Kishwaukee Bridge from global and local deformation measurements. Smart Structures and Materials (2004) Sensors and Smart Structures Technologies for Civil. Mechanical, and Aerospace Systems 5391:618. https://doi.org/10.1117/12.540215
37. National Bridge Inventory . 2018. "I-39 & US 51 NB over KISHWAUKEE RIVER." http://bridgereports.com/1161852
38. Holt, John, Oguzhan Bayrak, Pinar Okumus, Andreas Stavridis, Thomas Murphy, Dhaval Panchal, Animesh Dutta, and Akshay Randiwe. *Concrete Bridge Shear Load Rating Guide and Examples: Using the Modified Compression Field Theory*. No. FHWA-HIF-22–025. United States. Federal Highway Administration, 2022.
39. Glisic, B. (2011). Influence of the gauge length on the accuracy of long-gauge sensors employed in monitoring of prismatic beams. *Measurement Science and Technology*, *22*(3). https://doi.org/10.1088/0957-0233/22/3/035206
40. American Association of State Highway and Transportation Officials, A. (2017). *AASHTO LRFD Bridge Design Specifications.* Washington, D.C.
41. Barker, R. M. (Richard M.), & Puckett, J. Alan. (2007). *Design of highway bridges : an LRFD approach*. John Wiley & Sons.
42. Vecchio FJ, Collins MP (1986) The modified compression-field theory for reinforced concrete elements subjected to shear. ACI J 83(2):219–231
43. Walraven JC (1981) Fundamental analysis of aggregate interlock. J Struct Div 107(11):2245–2270
44. Collins MP, Mitchell D, Adebar P, Vecchio FJ (1996) A general shear design method. ACI Struct J 93(1):36–45